DEVELOPMENT OF AN ELECTRO-PNEUMATIC SERVO CLUTCH AND INDUSTRY-LEVEL CONTROLLER

by

TIMOTHY STEVENS

Presented to the Faculty of the Graduate School of

The University of Texas at Arlington in Partial Fulfillment

of the Requirements

for the Degree of

MASTER OF SCIENCE IN MECHANICAL ENGINEERING

THE UNIVERSITY OF TEXAS AT ARLINGTON

May 2022

Acknowledgements

I wish to thank Dr. Woods for his support. He has been a wonderful mentor and has taught me volumes. He has provided any resource or advice I could ask for and has provided an atmosphere to freely learn. His enthusiastic personality and unique perspective have made the project more fun than it should have been. His guidance has left a lasting impact which will be remembered.

I wish to thank my parents and my family. Each of you has encouraged me to follow my passion and supported me within your means. Without this support, I would be unable to aspire for more.

I wish to thank my friends, past and present, on the FSAE team. It has been a pleasure to know and work with such intelligent minds. You have taught me how effective and enjoyable good teamwork can be.

I wish to thank Michael Baldwin and his peers at SMC for providing the various pneumatic and sensing equipment necessary to make this project successful.

I also wish to thank my committee members, Dr. Robert Woods, Dr. Raul Fernandez, and Dr. Panos Shiakolas for taking the time to serve on my graduate committee and investing in me.

April 25th, 2022

Abstract

DEVELOPMENT OF AN ELECTRO-PNEUMATIC SERVO CLUTCH AND INDUSTRY-LEVEL CONTROLLER

Timothy Stevens, MS

The University of Texas at Arlington, 2022

Supervising Professor: Dr. Robert L. Woods

This thesis covers the simulation and development of an electro-pneumatic servo clutch used on an FSAE racecar. This project utilizes a sophisticated simulation and various techniques to increase performance such as utilizing pulse-width and pulse-frequency modulation and the use of a 36V supply with constant current limiting to drive the solenoids. The clutch is actuated using a pneumatic cylinder with the internal pressure modulated using commercially available CNG fuel injectors.

This thesis also describes the development of the electronic controller designed using analog circuits, as well as the integration of digital circuits to control operations such as launch control and half-shifts into the neutral gear.

Reliability and consumer-level-integration are both key priorities, thus all necessary components for the paddle-shifter system are designed into robust and convenient assemblies which can easily be packaged on a racecar with severe space limitations.

Integration of the pneumatic shifting and servo clutch allows for increased acceleration performance and less driver distraction during dynamic events.

Table of Contents

List of Illustrations

List of Symbols

Symbol	Units	Description
A	mm^2	Area
β	U.D.	Transistor Gain
C	mm^3	Upswept Volume of Actuator and Line Volume
C_d	U.D.	Discharge Coefficient
DC	U.D.	Duty Cycle
e	U.D.	Error Value
F	N	Force
f	Hz	Frequency
f_c	N	Static Coulomb Friction
G	U.D.	Gain
h	W/m^2K	Convection Coefficient
I	amperes	Current
K	U.D.	Gain Constant
k	N/mm or U.D.	Spring Constant or Heat Capacity Ratio
L	henry	Inductance
m	kg	Mass
n	kg/s	Injector Gain
P	kPa	Pressure
δP	kPa	Pressure Differential
R	ohm or Nm/kgK	Resistor or Ideal Gas Constant
r	mm	Radius
T	K	Temperature
τ	seconds	Time Constant
u	mm	Input
V	volt or mm^3	Voltage or Volume
x	mm	Injector Shuttle Position
z	mm	Actuator Position
θ	deg	Angle

List of Subscripts

Subscript	Description
abs	Absolute Value
$annular$	Annular
atm	Atmosphere
B	Base Terminal of a Transistor
BE	Between the Base and Emitter Terminals of a Transistor
c	Collector
cc	Supply
$crit$	Critical
cv	Control Volume
cyl	Cylinder
D	Derivative
d	Downstream
$Duty$	Duty Cycle
EM	Electromagnetic
$error$	Error
f	Frictional
fb	Feedback
$fb, scaled$	Scaled Feedback
$gear$	Gear
in	Entering the system
$inPot$	From Input Potentiometer
L	Inductor
min	Minimum
o	Summed Voltage of P and D Signals
$orifice$	Orifice
P	Proportional
p	Preload
r	Ratio
sat	Saturation
set	Set Point for Constant Current or Relating to PWM Frequency of LTC6992
$shut$	Shuttle
u	Upstream
w	Pertaining to the inside surface of the actuator
Z	Zener

Chapter 1: Introduction

This chapter describes the relevance of this project and the solutions the UTA FSAE team has used in the past. It also discusses the basic system architecture, and why a paddle-shifter system is advantageous.

1.1 FSAE Competition

The FSAE competition is a collegiate competition involving the construction and racing of student-designed racecars. These cars weigh approximately 450 pounds, produce about 70 horsepower, and compete on a course where maximum speeds are about 60 mph. Competitiveness among student teams is maintained by following a strict rulebook. There are over 800 teams competing around the world. In the competition, teams must compete in four dynamic events: acceleration, skidpad, autocross, and endurance.

The acceleration event is a timed 250 foot long straight which a driver must accelerate through from a stop. The skidpad event measures the lateral G capacity of the car/tires and is not relevant to this paper. The autocross event is a timed course of mixed acceleration, turning, and braking. The endurance event is 13.7 miles of continuous autocross driving, with a driver change halfway. The dynamic events consist of 68% of the total score at the competition.

The electro-pneumatic paddle-shifter system described within was prototyped and developed on the UTA 2018 car, which features a Honda CBR600RR motorcycle engine. The final version of the paddle-shifter controller is designed for the UTA 2022 car which features a turbocharged Yamaha R3 engine. Additional calculation was performed to prepare for implantation on various engines, such as the Yamaha YZF450F, and Honda CBR600F4I.

1.2 UTA Hand Clutch

The pre-existing clutch/shifter design is purely mechanical. It consists of two levers attached to a common base which is allowed to rotate on a fixed pivot. When the levers are

squeezed together, the clutch is pulled in. When the entire assembly is rotated, the engine is shifted. This allows for “one-touch” operation, meaning the operation of this shifter on track requires only a push forwards or a pull backwards. The clutch operates automatically during downshifts based on a force ratio and upshifts occur without the use of a clutch. It is a simple and brilliant design which UTA has used since 1985.

Fig. 1-1 UTA Manual Shifter Configuration, 1985-Present

This design is not, however, perfect. Sizable packaging accommodations must be made during the design of the car, specifically behind the driver and next to the fuel tank. Furthermore, adaptation of this shifter is not convenient on some engines which have been modified. Turbocharged engines sometimes require stiffer aftermarket clutch springs to prevent clutch slip and can have an extremely stiff clutch. To accommodate this, the shifting force must increase, or the overall stroke of the shifter must be increased. This makes the use of a mechanical system inconvenient due to either too much stroke or too high of a force.

1.3 My Contribution

This project is a continuation of the results from a thesis completed by Rahul J. Chalmela in 2017 [3]. His project produced the first prototype of this paddle-shifter system with ample need for improvement. There was no simulation performed, thus there is great opportunity for refinement, both in performance and efficiency. The prototype controller had its limitations as well; only a handful of PWM frequencies could be chosen to drive the injectors, thus a precise frequency could not be selected. The digital PWM control also had some latency issues which made the clutch response feel unstable. Furthermore, there is need for a robust controller which integrates elegantly into an FSAE car with mitigated potential for failure.

This thesis addresses these issues. A simulation of the injectors and paddle-shifter system is performed to evaluate the effect of various parameters on performance. An analog controller is designed which minimizes latency from approximately 30ms to less than 6ms. This controller also varies the PWM frequency automatically. The new controller and implementation of the paddle-shifter system allows for faster and smoother actuation of the clutch. The previous system lags a ramp input by approximately 100ms, while my new system lags by approximately 50ms.

1.4 Engine Internals

A motorcycle transmission is sequential. On the majority of engines, a splined shifter shaft exits the engine. Rotating this clockwise upshifts, and counterclockwise downshifts (or vice-versa depending on the engine). On the inside of the engine is a mechanism which requires the shaft to return to its middle position to perform an additional shift. An additional quirk of this mechanism is that the shifter can be held in one direction following a shift without consequence.

Fig. 1-2 Engine Shifter Ratcheting mechanism

It is necessary in most engines for the transmission gears to be briefly unloaded for the shift to actuate, otherwise there is too much friction for the foot, or in this case pneumatic cylinder, to overcome. This is why cutting the ignition during shifts is critical: to unload the transmission and allow it to shift. Given the properties of the shifter mechanism, the "shift time" is not how long the cylinder is extended, it is how long the ignition is cut. The controller program leaves the cylinder extended for approximately 80ms beyond the conclusion of a shift, simply to ensure the shift is successful.

A motorcycle clutch is typically a multi-plate wet clutch internal to the engine casing. This wet clutch is actuated by a rod through the center of the clutch, and a lever embedded in the side cover. By contrast, this mechanism is much simpler, and a linear relationship between clutch engagement and rotation of the clutch shaft can be assumed.

1.5 Quantified Benefit of Faster Shift Times

As mentioned previously, there are four dynamic events in the FSAE competition: acceleration, skidpad, autocross, and endurance. Skidpad will see no benefit or deficit from the shifting system. Acceleration, however, will see the most obvious and quantifiable benefit.

In a typical acceleration event, a FSAE car will shift about two times. From analyzing on-track data, it has been found that the mechanical shifter accomplishes upshifts in a minimum of 150ms, while the paddle-shifters accomplish an upshift consistently in 50ms. A shorter shift time means the engine will deliver more energy into the car and will cover the required distance over a shorter period of time. The paddle-shifters allow for approximately 5% more time to deliver this energy.

A benefit gained at an autocross or endurance event is more difficult to quantify. There are straight sections where you could consider the time saved by each shift, just as above, however one could argue that driver variance will account for more time than the aforementioned margin. Which is, coincidently, the largest selling point for paddle-shifters: assisting the driver. Some claim that keeping the driver's hands on the same points of the steering wheel is easier. Some claim that the instantaneity of the shifting allows drivers to shift in situations where they normally wouldn't be able to. Some claim that having a reliable shift and not having to blip the throttle would keep the driver focused. These are, however, subjective measures and could easily be disputed. If a driver weren't to agree with any of these arguments, the system would still perform as good or better than a mechanical shifter, with the only cost being the risk of unreliability. It is therefore likely the paddle-shifter system will outperform the mechanical shifter.

1.6 Possibilities for Launch Control

Once the clutch is controlled electronically, a reliable launch control can be implemented. This control would be strictly passive. Active control, which responds to wheel slip, would need to implement an electronic throttle or some other responsive power-cutting device. Active control with clutch actuation would surely overheat the clutch plates. A passive control, however, can be almost as good.

This system works as follows: First, the driver pulls in the clutch and engages the launch button. This moves the clutch to a position just before the bite point. It also engages a secondary RPM limit within the ECU. Upon releasing the button, the paddle shifter controller will release the clutch at a constant rate. The RPM limit will be released at some

point within this process. The throttle position, and thus the engine manifold pressure, just before the car is launched will define the initial severity of the launch and can be used to accommodate for various surfaces. In this method, the driver needs to focus on far fewer variables. This provides a consistently fast launch.

Chapter 2: Analysis

This chapter describes the analysis and simulation development performed before a physical prototype can be constructed. A model of the fuel injectors used in the system is created first, which greatly simplifies the subsequent derivation and analysis of the system dynamics.

The electro-pneumatic servo clutch consists of a linear pneumatic actuator whose pressure is modulated using two CNG fuel injectors. The fuel injectors are used in leu of commercial pneumatic valves for their fast response time. The pressure is supplied by a regulated compressed air tank. A simplified view of this arrangement is shown in Fig. 2-1. The shifting system consists only of a valve and a two-position pneumatic cylinder, which requires only rudimentary analysis and will thus not be discussed in this section.

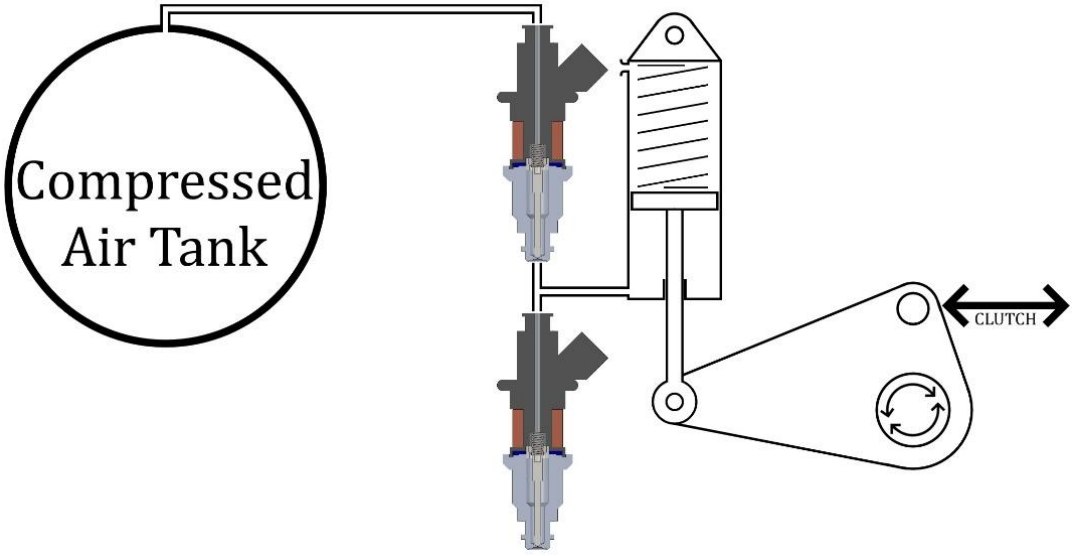

Fig. 2-1 Global System Overview

2.1 Lumped Spring and Mass Calculation

To make subsequent analysis more convenient, a lumped spring constant and a lumped mass is solved for from the system components. A summary of the spring rates and masses present for different engines is shown in Fig. 2-2. There are only two mechanical springs of interest in this system: The clutch springs internal to the engine and the spring

inside the pneumatic cylinder. The spring rate of the clutch has been measured for various engines by attaching a force gauge to the end of the engine clutch bellcrank. The spring rate of the pneumatic cylinder is listed on its datasheet [2]. The rotation of the bellcrank is assumed to modify the linearity of these springs a negligible amount.

Car		F18	F22	600f4i	YZF450
Clutch Torque	in-lbf	28	58	69	48
Clutch Angle	deg	12.4	16.5	17.6	12.0
Lever Arm	in	2.83	1.90	2.00	1.76
Clutch Rate	lbf/in	16.5	56.6	57.0	74.5
Cylinder		SMC NCDMC088-0100T			
Cylinder Rate	lbf/in	3	3	3	3
Internal Engine mass	lbm	1.55	1.21	1.55	1.21
Internal Lever Arm	in	0.24	0.31	0.24	0.31
External Mass	lbm	0.2	0.2	0.2	0.2
Lumped Spring Rate	lbf/in	19.5	59.6	60.0	77.5
Lumped Mass	lbm	0.331	0.397	0.386	0.413
Clutch stroke	in	0.62	0.56	0.63	0.37
Lumped Spring Rate	N/mm	3.4	10.5	10.5	13.6
Lumped Mass	kg	0.151	0.181	0.176	0.188
Clutch stroke	mm	16	14	16	10

Fig. 2-2 Lumped Mass and Spring Calculations

There are several masses of interest. The mass of the piston, bell crank, and internal engine pushrod must all be accounted for. Half of the weight of the clutch was included, since one side remains stationary, and the other moves the full stroke. The rotational inertia of the bellcrank is assumed negligible since it accounts for less than 5% of the total mass and its center of gravity is nearly at the rotation axis.

2.2 Fuel Injector Model

To develop a sufficient dynamic model of the system, the fuel injectors must be appropriately modeled. It is convenient to simplify the behavior of the injectors into a single variable which can be used in the full dynamic system model. This allows for faster iterations because it is not necessary to simulate an injector opening and closing possibly a few hundred times for each clutch actuation simulation. If this simplification is executed

properly, no simulation accuracy will be lost. This variable will convert the PWM duty cycle to mass flow and be called the injector gain.

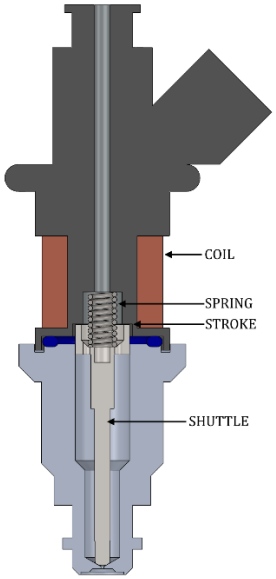

Fig. 2-3 Typical fuel injector cross section

Fig. 2-3 depicts a typical fuel injector cross section, consisting of a shuttle which seals an orifice, a preloaded spring to force the shuttle closed, and an electromagnetic coil. The shuttle sees forces from the spring, inertia, a pressure differential across the orifice, and the electromagnetic force, as described by equation 2.1.

$$f_{Inj.Force}(I_L, x(t)) = m\ddot{x}(t) + kx(t) + F_P + \delta P A_{orifice} \tag{2.1}$$

As the injector opens, the pressure differential across the shuttle reduces and becomes negligible. Furthermore, the mass flow of the injector will increase as the shuttle moves. From experience with fuel injectors, I know that the shuttle is only in this transition range for approximately 100µs, thus a linear approximation can be used without degrading accuracy. Therefore, a shuttle displacement x_{crit} is defined, where the pressure differential diminishes, and the mass flow changes. Over the range of zero displacement to x_{crit}, the normalized mass flow will linearly vary from 0 to 1. Beyond x_{crit} the normalized mass flow is 1. This relationship is shown in Fig. 2-4 and by equation 2.2.

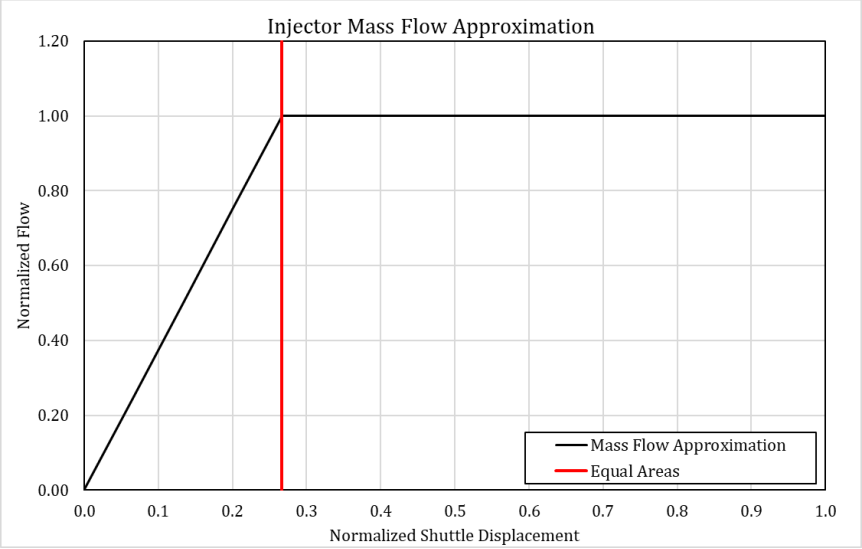

Fig. 2-4 Injector mass flow approximation

$$if\ x \le x_{crit}, \qquad \frac{\dot{m}}{\dot{m}_{max}} = 1 * \frac{x}{x_{crit}}$$
$$if\ x > x_{crit}, \qquad \frac{\dot{m}}{\dot{m}_{max}} = 1 \tag{2.2}$$

The height of x_{crit} is determined by when the orifice area is equal to the annular area between the shuttle and the sealing face. Geometry used to calculate this height is shown in Fig. 2-5. Calculations for x_{crit} and the two areas are shown by equations 2.3, 2.4, and 2.5.

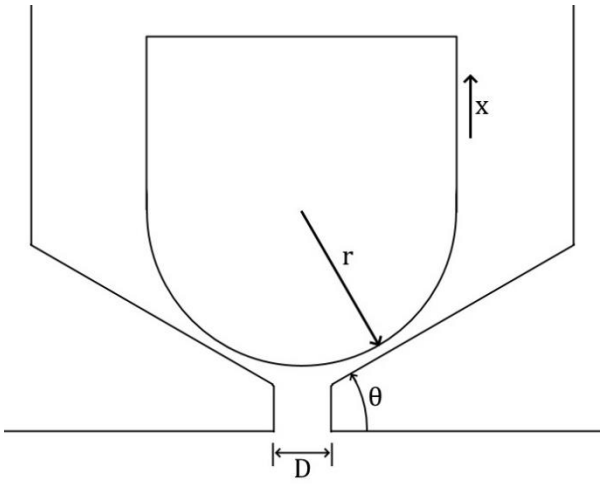

Fig. 2-5 Dimensions used for calculating annular area and critical shuttle height

$$A_{orifice} = \frac{\pi {D_{orifice}}^2}{4} \tag{2.3}$$

$$A_{annular} = \pi \sin^2 \theta_{shut} * (x^2 + 2x r_{shut}) \tag{2.4}$$

$$x_{crit} = \sqrt{\frac{{D_{orifice}}^2}{4 \sin^2 \theta_{shut}} + {r_{shut}}^2} - r_{shut} \tag{2.5}$$

To determine parameters of the components in the injector, one was carefully disassembled. The spring rate, shuttle mass, orifice dimensions, preload distance, and maximum travel were all found experimentally. Additionally, an expression for the electromagnetic force was developed from experimentally collected data. These processes are described in greater detail in Appendix B. The linearized electromagnetic force model is shown in Fig. 2-6 and by equations 2.6, 2.7, and 2.8.

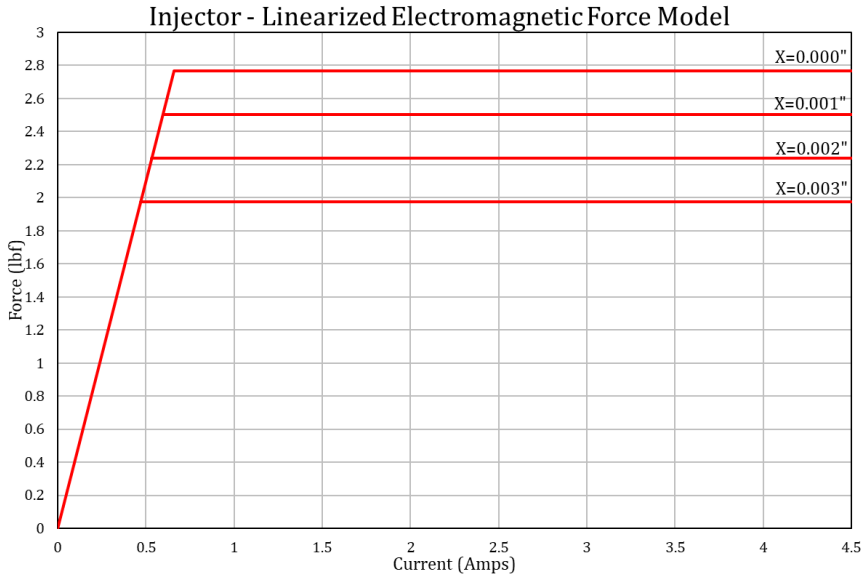

Fig. 2-6 Linearized Electromagnetic Force Model

$$F_{inj.Force} = 4.2 \frac{lb_f}{A} * I_L \tag{2.6}$$

$$F_{inj.Force,saturate} = -263.8 \frac{lb_f}{inch} * x + 2.8\ lb_f \tag{2.7}$$

$$4.2 \frac{lb_f}{A} = 18.7 \frac{N}{A}, \qquad 263.8 \frac{lb_f}{inch} = 46.2 \frac{N}{mm}, \qquad 2.8\ lb_f = 12.5\ N \tag{2.8}$$

The 2nd order mechanical dynamics ODE, given by equation 2.1, only applies when the injector stroke is greater than zero but less than the maximum stroke. At either mechanical limit, the shuttle will stop, and the velocity will go to zero. This collision is assumed to be completely inelastic and is represented by equations 2.9 and 2.10. These equations are essentially extremely fast decays. Using a decay too fast, however, can make the simulation take longer to solve, thus it is advantageous to decay as slow as possible while maintaining accuracy. The rate of decay was determined by iterating the simulation, progressively making the decay slower, until the decay took a significant amount of time relative to the mechanical dynamics depicted by equation 2.1.

$$\dot{x}(t) = 10(x_{max} - x(t)) \tag{2.9}$$

$$\ddot{x}(t) = -1000000\dot{x}(t) \tag{2.10}$$

The electrical dynamics is a simple 1st order ODE derived from the current flow through an RL circuit shown in Fig. 2-7. The electrical dynamics is shown in equations 2.11 and 2.12.

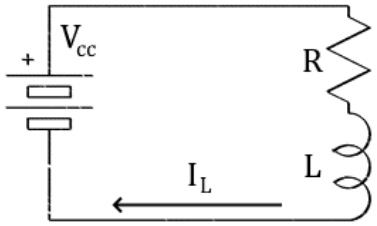

Fig. 2-7 Simplified Injector Schematic

$$I_L(t) = \frac{\frac{1}{R}V_{cc}}{1 + \frac{L}{R}D} \tag{2.11}$$

$$\dot{I_L}(t) = \frac{V_{cc} - I_L(t) * R}{L} \tag{2.12}$$

The resistance could include the source resistance (in this case the battery ESR and the wire resistance) and the injector resistance, however the source resistance is assumed to be negligible relative to the injector resistance.

The model for the injector turning off depends on the flywheel diode configuration. The common solution of a single diode across the inductor will have a slow current decay. The circuit which will be used for this controller will have a flywheel and zener diode, which provides a much faster current decay while avoiding extreme voltage spikes which damage components. The current decay is assumed instant using the equation 2.13. The rate at which this equation decays was found in the same method as discussed for equations 2.9 and 2.10.

$$\dot{I_L}(t) = -1000000 * I_L(t) \tag{2.13}$$

If a constant current regulator is used to drive the injector, equation 2.14 will apply while the input signal is high and the current from the first equation is greater than the set current:

$$\dot{I_L}(t) = 1000000 * (I_{set} - I_L(t)) \tag{2.14}$$

A constant current regulator can be very useful to improve electrical efficiency and heat dissipation in the injector. Furthermore, if a higher voltage than what the injector was designed for is utilized, a much better transient performance can be achieved.

Equations 2.1 and 2.12 are converted to a state variable representation and shown by equations 2.15, 2.16, and 2.17.

$$x_1 - Shuttle\ Position$$
$$x_2 - Shuttle\ Velocity$$
$$x_3 - Coil\ Current$$

$$Dx_1 = x_2 \tag{2.15}$$

$$Dx_2 = \frac{1}{m}\left(kx_1 + F_p + \delta PA_{orifice} - f_{Inj.Force}(I, x)\right) \tag{2.16}$$

$$Dx_3 = \frac{V_{cc} - x_3 R}{L} \tag{2.17}$$

2.3 Injector Output Summary

Using the equations derived in section 2.2, the injector output can be simulated. Fig. 2-8 depicts a simulation of the injector operating at 200Hz, 50% duty cycle. It is being driven by a 12 volt source with a constant current limiter.

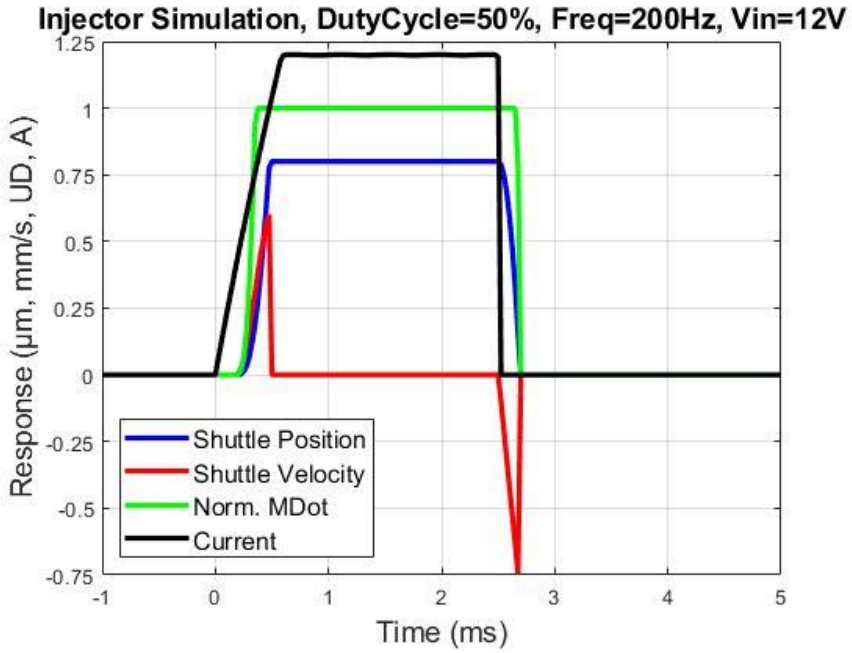

Fig. 2-8 Injector Response

This simulation is not accurate for estimating mass flow at large duty cycles. This is because the simulation assumes zero initial conditions. At duty cycles larger than ~90%, the mechanical state variables may be non-zero at the beginning of the subsequent PWM cycle. For the following cycles, the injector is open longer than the initial cycle which is simulated. Linear behavior will be assumed until 100% duty cycle.

What is more important is the injectors behavior at small duty cycles, about 10% or less. This will determine the minimum deadband of the controller. Furthermore, any error perceived by the controller which stays in this range where no mass flow is created will be continuously sending a small amount of current through the injector which may cause thermal issues over time.

In Fig. 2-9, the simulation is performed again with a higher supply voltage. The current rise time is greatly improved. This will be an important factor towards mitigating the minimum duty cycle.

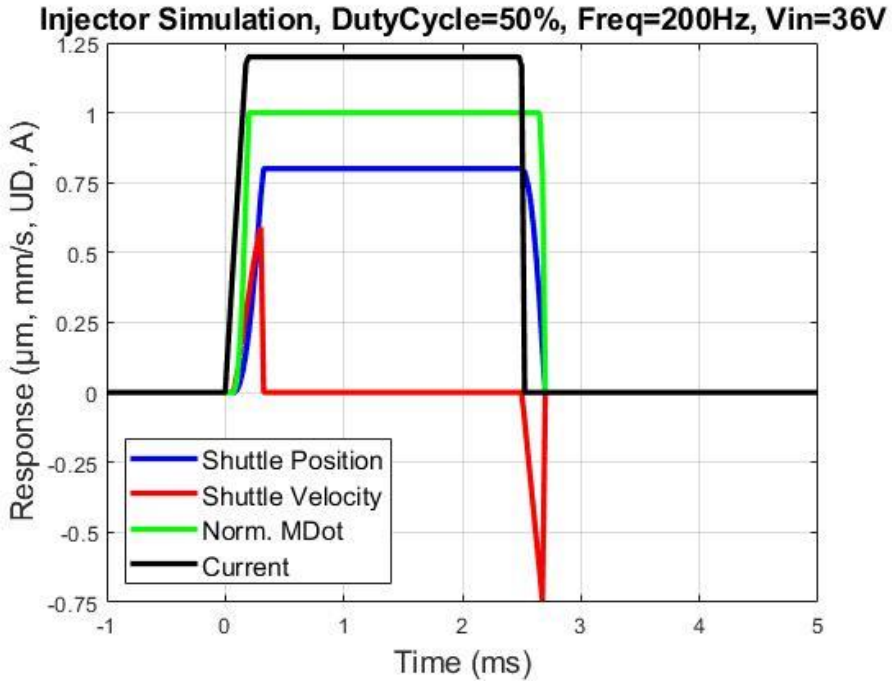

Fig. 2-9 High Supply Voltage Injector Response

If this simulation is run for the entire range of duty cycles and the average mass flow is recorded, an input/output plot can be developed, shown in Fig. 2-10. This injector gain is analogous to electrical transconductance.

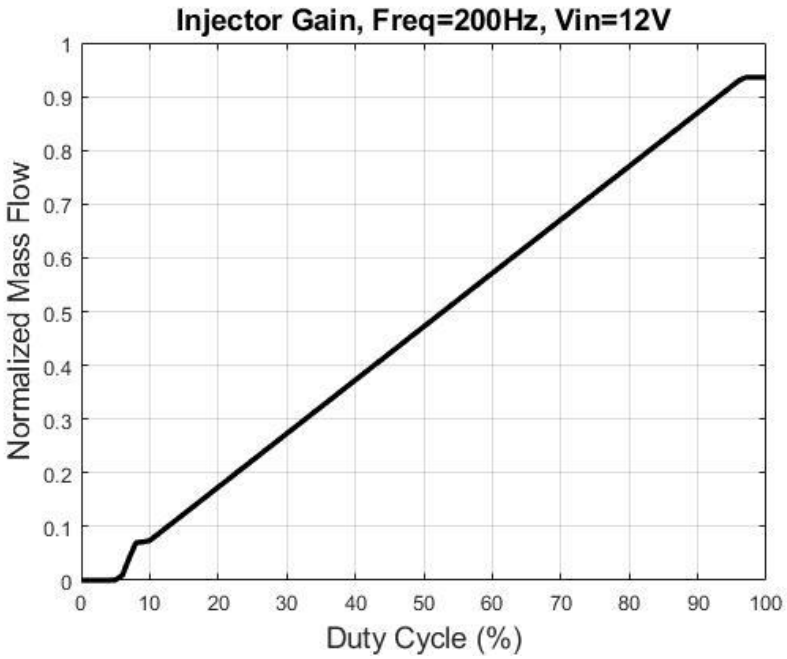

Fig. 2-10 Injector Gain, 200Hz, 12V

The discontinuities at low duty cycles are notable. The first one, which initially creates mass flow, is a function of the electrical current rise mode and the shuttle position mode. This means there will be diminishing returns in reducing this minimum duty cycle by improving the electrical rise time, as the mechanical dynamics become the dominate mode.

The second discontinuity, where the mass flow briefly peaks higher than the linear trend is caused by the assumption of a completely inelastic collision between the shuttle and the injector body. This duty cycle causes the shuttle to rise but not quite touch the upper stop. Thus, the shuttle does not lose as much energy as if it had contacted the stop. The position and velocity of the shuttle must then decay through the second order equations, which are slower than the equations which describe the inelastic collision. A simulation of this discontinuity is shown in Fig. 2-11. Observe how the shuttle position and velocity decays slower than that shown in Fig. 2-8.

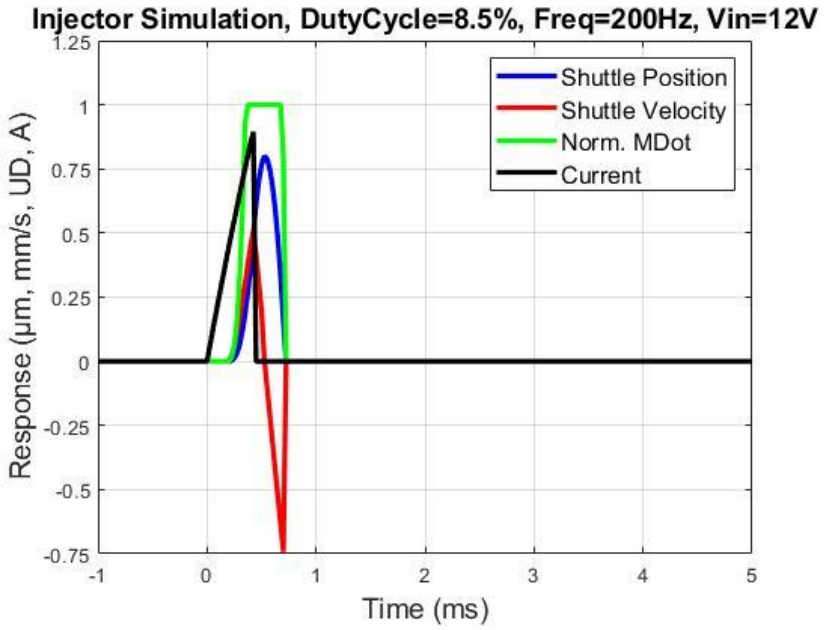

Fig. 2-11 Small Duty Cycle Discontinuity Response

To summarize the performance of various configurations, an average gain and minimum duty cycle can be defined for each. Simulations were run for 12V, 24V, 36V, 48V, and 60V at 200Hz. Additionally, the minimum duty cycle was recorded for each voltage at 60Hz.

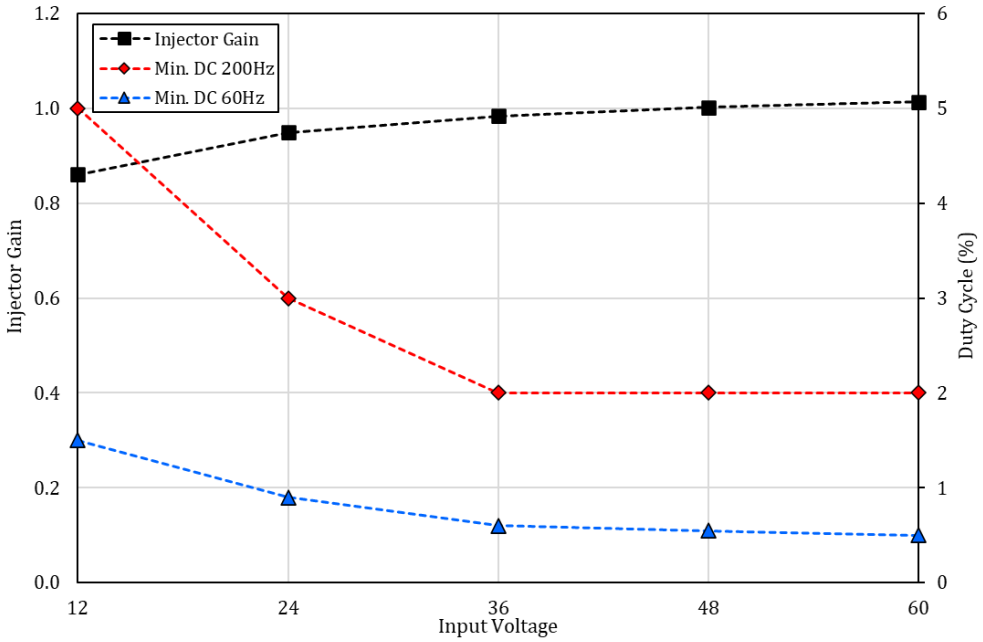

Fig. 2-12 Injector Gain and Minimum Duty Cycle Summary

In Fig. 2-12, diminishing returns are observed beyond 36 volts, where the mechanical dynamics dominate the system response. A lower supply voltage is advantageous as this will produce less heat when in constant current operation. A 36 volt supply offers nearly equivalent performance as higher supply voltages and will be used to drive the injectors.

Decreasing the PWM frequency will reduce the minimum duty cycle because the constraint for the injector opening is actually a minimum pulse width. However, operating at higher frequencies provides improved controller responsiveness. Thus, the PWM frequency can be changed as a function of the duty cycle. At small duty cycles, where precision is important, a low frequency will be used. At higher duty cycles, a faster frequency will be used. The PWM frequency will vary linearly as a function of the duty cycle, from 60Hz to 500Hz. This frequency range is selected based on the adjustment range available from the LTC6992-1 IC used to generate the PWM signal.

Varying the frequency and duty cycle in this manner is similar to a bang-bang or PWFM (Pulse Width Frequency Modulation) controller but has the advantage of not requiring hysteresis.

Implementing the frequency modulation in our simulation provides the final output function shown in Fig. 2-13 and characterized by equation 2.18. Minimum duty cycle is measured as 0.6%, and the average gain is 1.01.

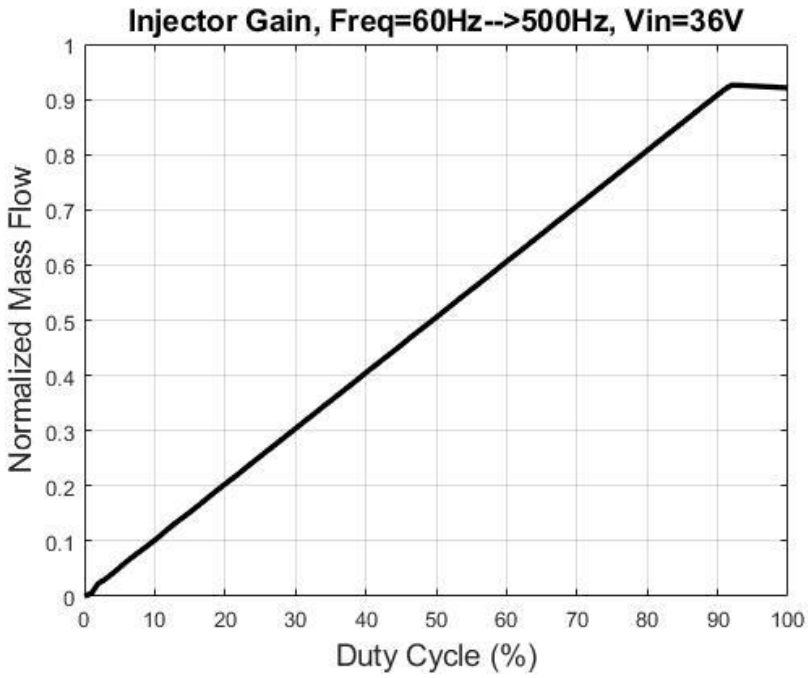

Fig. 2-13 Injector Output with Frequency Modulation

$$\begin{aligned} if\ DC < 0.6\%, n &= 0 \\ if\ DC \geq 0.6\%, \quad n &= 1.01 * DC \\ if\ n > 1, n &= 1 \end{aligned} \tag{2.18}$$

2.4 Dynamic Model

The connection from the compressed air tank and the first injector is accomplished using a relatively large ¼" pneumatic line, thus the source impedance between the regulator and the first injector is assumed to be negligible relative to the injector impedance. Furthermore, the vent orifice on the open side of the cylinder is assumed to be large enough that its impedance is also negligible.

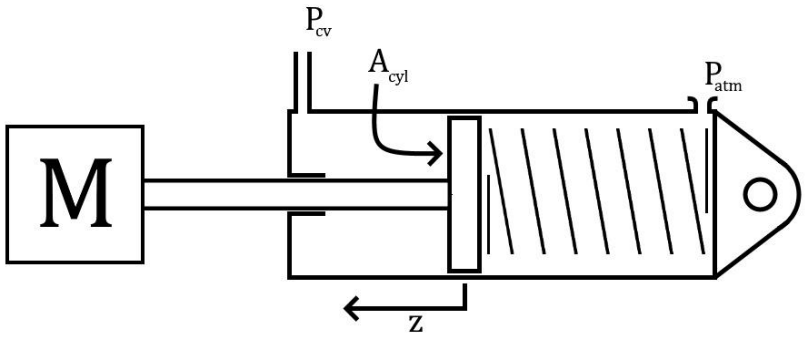

Fig. 2-14 Piston force and flow balance

The force balance at the piston of the cylinder is shown in Fig. 2-14 and given by equation 2.19.

$$(P_{cv}(t) - P_{atm})A_{cyl} - kz(t) - m\ddot{z}(t) - F_f(\dot{z}(t)) = 0 \tag{2.19}$$

$F_f(\dot{z}(t))$ is a frictional force function representing coulomb friction in the cylinder. This function is described in detail in Appendix A. The spring rate and mass are modeled as lumped sums, as shown in section 2.1. By using these lumped sums, an additional equation describing the rotation of the bellcrank can be avoided. We will also require a flow balance at the cylinder, shown by equations 2.20, 2.21, and 2.22. The variable C represents the un-swept volume.

$$V_{cv}(t) = A_{cyl}z(t) + C \tag{2.20}$$

$$\dot{V}_{cv}(t) = A_{cyl}\dot{z}(t) \tag{2.21}$$

$$M_{cv}(t) = \frac{P_{cv}(t)V_{cv}(t)}{RT_{cv}(t)} \tag{2.22}$$

Mass flow through an orifice is described by equation 2.23 [10].

$$\dot{m} = C_d A * P_u \sqrt{\frac{2}{RT_d}} * \sqrt{P_r - P_r^2}, \qquad where\ P_r = \frac{P_d}{P_u}, \qquad if\ P_r < 0.5, then\ P_r = 0.5 \tag{2.23}$$

Applying equation 2.23 to the two injectors yields equations 2.24 and 2.25. Note that a variable "n" is placed at the beginning of this expression, and accounts for the injector gain found in section 2.3. These equations are accompanied by the condition that $\dot{m}_{in}$ is nonzero only when n>0, and $\dot{m}_{out}$ is nonzero only when n<0.

$$\dot{m}_{in}(t) = n(t)C_d A * P_u \sqrt{\frac{2}{RT_d(t)}} * f_{pr\_up}, \qquad f_{pr\_up} = \sqrt{\frac{P_{cv}(t)}{P_u} - \left(\frac{P_{cv}(t)}{P_u}\right)^2} \tag{2.24}$$

$$\dot{m}_{out}(t) = n(t)C_d A * P_{cv}(t) \sqrt{\frac{2}{RT_{atm}}} * f_{pr\_dn}, \qquad f_{pr\_dn} = \sqrt{\frac{P_{atm}}{P_{cv}(t)} - \left(\frac{P_{atm}}{P_{cv}(t)}\right)^2} \tag{2.25}$$

To properly simulate the dynamic response of this pneumatic system, equations 2.26 and 2.27 [11] will be required. These equations are derived from the first law of thermodynamics and represent pressure and temperature as state variables.

$$\frac{\frac{d}{dt}P_{cv}(t)}{P_{cv}(t)} = k\left[\frac{\dot{m}_{in}(t)}{M_{cv}(t)}\frac{T_{in}}{T_{cv}(t)} - \frac{\dot{m}_{out}(t)}{M_{cv}(t)}\right] - \frac{(k-1)}{P_{cv}(t)V_{cv}(t)}(T_{cv}(t) - T_w)hA_w - k\frac{\frac{d}{dt}V_{cv}(t)}{V_{cv}(t)} \tag{2.26}$$

$$\frac{\frac{d}{dt}T_{cv}(t)}{T_{cv}(t)} = \frac{\dot{m}_{in}(t)}{M_{cv}(t)}\left[k\frac{T_{in}}{T_{cv}(t)} - 1\right] - \frac{\dot{m}_{out}(t)}{M_{cv}(t)}[k-1] - \frac{(k-1)}{P_{cv}(t)V_{cv}(t)}(T_{cv}(t) - T_w)hA_w - (k-1)\frac{\frac{d}{dt}V_{cv}(t)}{V_{cv}(t)} \tag{2.27}$$

The last equation necessary is one to represent the controller. A PD controller is represented by equation 2.28.

$$e(t) = K_P(u(t) - z(t)) + K_D(\dot{u}(t) - \dot{z}(t)) \tag{2.28}$$

The controller output must be saturated at 100% duty cycle. This condition is shown by equation 2.29.

$$if: \begin{cases} e(t) > 1 \\ -1 \le e(t) \le 1, \\ e(t) < -1 \end{cases} \qquad then: \begin{cases} DC(t) = 1 \\ DC(t) = e(t) \\ DC(t) = -1 \end{cases} \tag{2.29}$$

2.4.1 Converting to a State Variable Representation

This system has four state variables described below. Equations 2.30-2.33 depict their behavior. Unit conversions are supplied to maintain unit consistency.

$$x_1 - Piston\ Position$$
$$x_2 - Piston\ Velocity$$
$$x_3 - Cylinder\ CV\ Pressure$$
$$x_4 - Cylinder\ CV\ Temperature$$

$$Dx_1 = x_2 \tag{2.30}$$

$$Dx_2 = \frac{1}{m}\left((x_3 - P_a)A_{cyl} - kx_1 * \frac{1000mm}{1m} - F_f(\dot{z}) * \frac{1000mm}{1m}\right) \tag{2.31}$$

$$\frac{Dx_3}{x_3} = k\left[\frac{\dot{m}_{in}}{M_{cv}}\frac{T_a}{x_4} - \frac{\dot{m}_{out}}{M_{cv}}\right] - \frac{(k-1)(x_4 - T_w)hA_w}{x_3 V_{cv}} - k\frac{\dot{V}_{cv}}{V_{cv}} \tag{2.32}$$

$$\frac{Dx_4}{x_4} = \frac{\dot{m}_{in}}{M_{cv}}\left[k\frac{T_a}{x_4} - 1\right] - \frac{\dot{m}_{out}}{M_{cv}}[k-1] - \frac{(k-1)(x_4 - T_w)hA_w}{x_3 V_{cv}} - (k-1)\frac{\dot{V}_{cv}}{V_{cv}} \tag{2.33}$$

Mass flow equations are given by equations 2.34, 2.35, and 2.36.

$$if\ DC > 0, then \qquad \dot{m_{in}} = \frac{1m}{1000mm} * nC_d A * P_u \sqrt{\frac{2}{Rx_4}} * f_{pr_{up}}, else \qquad \dot{m_{out}} = 0 \tag{2.34}$$

$$if\ DC < 0, then \qquad \dot{m_{out}} = \frac{1m}{1000mm} * nC_d A * x_3 \sqrt{\frac{2}{RT_a}} * f_{pr_{dn}}, else \qquad \dot{m_{in}} = 0 \tag{2.35}$$

$$f_{pr\_up} = \sqrt{\frac{x_3}{P_u} - \left(\frac{x_3}{P_u}\right)^2}, \qquad f_{pr\_dn} = \sqrt{\frac{P_a}{x_3} - \left(\frac{P_a}{x_3}\right)^2} \tag{2.36}$$

Supporting variables are given by equations 2.37, 2.38, and 2.39.

$$V_{cv} = A_{cyl}x_1 + C \tag{2.37}$$

$$\dot{V_{cv}} = A_{cyl}x_2 \tag{2.38}$$

$$M_{cv} = \frac{1m^2}{1{,}000{,}000mm^2} * \frac{x_3 V_{cv}}{Rx_4} \tag{2.39}$$

2.5 MATLAB Simulation

A digital simulation will allow for investigation into changing various parameters without the monetary or time investment of physical prototyping. Certain refinements can be evaluated which may increase system performance, reduce weight, or improve manufacturability.

Stability is paramount. The clutch position must not have any high frequency modes and minimal oscillations. The response should be primarily overdamped. Responsiveness will also be important, in this case evaluated as the settling time for a step input, or the steady state error for a ramp input. The system operates at a relatively high frequency compared to the user input frequency; thus, a ramp-step input will be our primary metric. The benchmark speed will be a FSI (full scale input) of 16mm in 500ms: this is about the average speed the user will use. A step input will be used to represent extremely fast inputs and ensure worst-case stability.

A PD controller was selected after some simulation results revealed the need for greater system dampening. This is obvious when considering the only speed-based-force is the friction within the cylinder.

Tuning of the proportional and derivative gains was conducted loosely following the procedure outlined for tuning a lead compensator via frequency response in *Control Systems Engineering* [6]. First, with the derivative gain set to zero, the proportional gain was increased until oscillations became evident, depicting a phase margin of approximately 20°. Then, the derivative gain was increased until the oscillations disappeared, and the output became stable and predominately overdamped. This yielded a proportional gain of 0.75 and a derivative gain of 0.025.

A true derivative circuit is not realistic to implement, especially on a racecar. Automobiles in general are laden with massive amounts of electrical noise. Most of this noise comes from the engine electronics and pumps. It is necessary, then, to utilize a bandwidth-limited differentiator and several filters to remove high frequency components, as well as using shielded wiring for the position and input signals. For electrical convenience, as will be described in chapter 3, two first order low pass filters with the

same cutoff frequency will be used in series. This transforms the PD controller equation into equation 2.40.

$$e(t) = K_P(u(t) - z(t)) + \frac{K_D(\dot{u}(t) - \dot{z}(t))}{(\tau_i(\dot{u}(t) - \dot{z}(t)) + 1)(\tau_1(\dot{u}(t) - \dot{z}(t)) + 1)^2} \tag{2.40}$$

Generally, to avoid reducing performance, the filter frequencies should be at least an order of magnitude greater than the K_D frequency. All three of the filter poles are ten times this frequency, at 63Hz. This arrangement of filters was found to be an acceptable tradeoff between performance and noise attenuation. If too much noise is present in the error signal, the derivative circuit can be disabled, although the proportional gain must be turned down and the system performance will suffer.

2.5.1 Ramp Input Responses

The tuned system response to a FSI/500ms ramp-step is shown in Fig. 2-15. The position lags the input by 47ms in the ramp range.

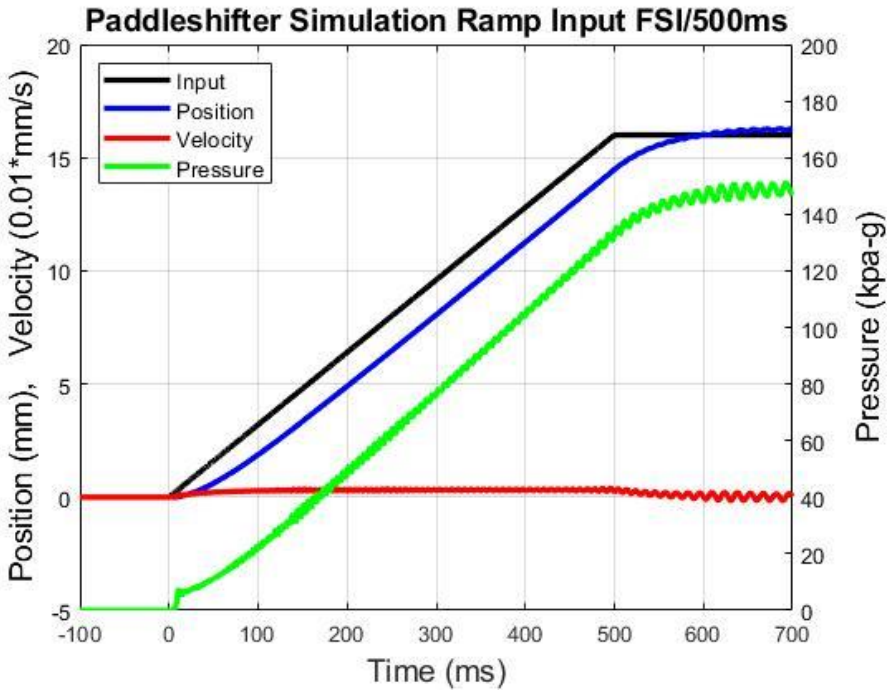

Fig. 2-15 Ramp-Step Response FSI/500ms

There are notable oscillations in the velocity, pressure, and temperature traces at high positions. This is caused by the control volume increasing creating a larger pneumatic capacitance between the injector and the piston. This can be observed by increasing the un-swept volume, i.e., the volume of air in the pneumatic lines. The simulation shown in Fig. 2-15 assumes the injectors are mounted directly to the cylinder with a volume of 900mm^2. If 700mm of 2mm ID pneumatic line is added between the cylinder and injectors, this volume becomes 2900mm^2. This simulation is shown is shown in Fig. 2-16.

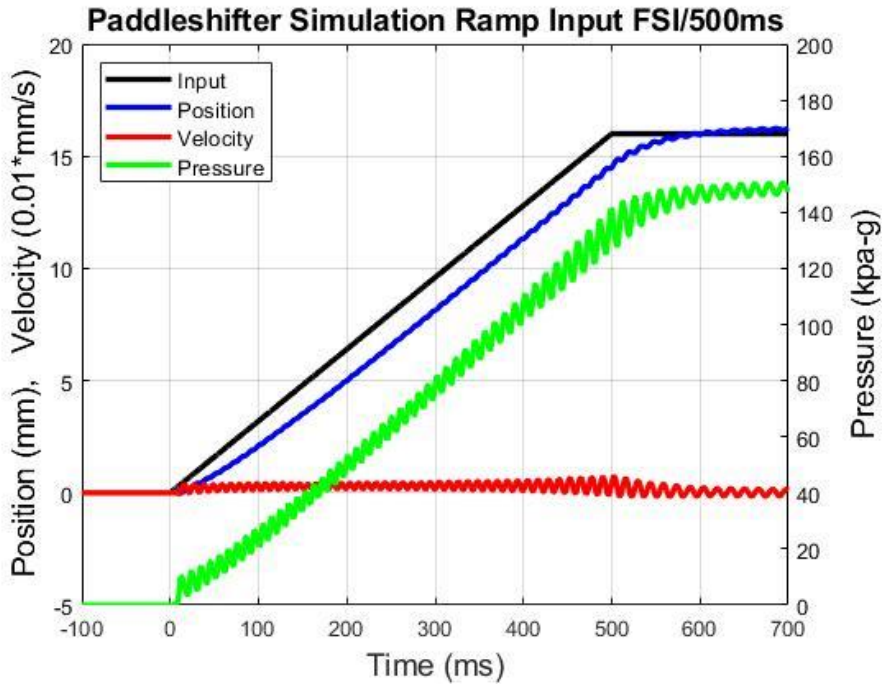

Fig. 2-16 Ramp-Step Response FSI/500ms with line capacitance.

In this simulation, the oscillations are greater across the entire range of travel but are especially higher at ranges where there is high controller command. Obviously, the derivative gain could be increased to alleviate these oscillations, but the step input rise time and steady state ramp error would suffer. However possible, the line capacitance should be minimized.

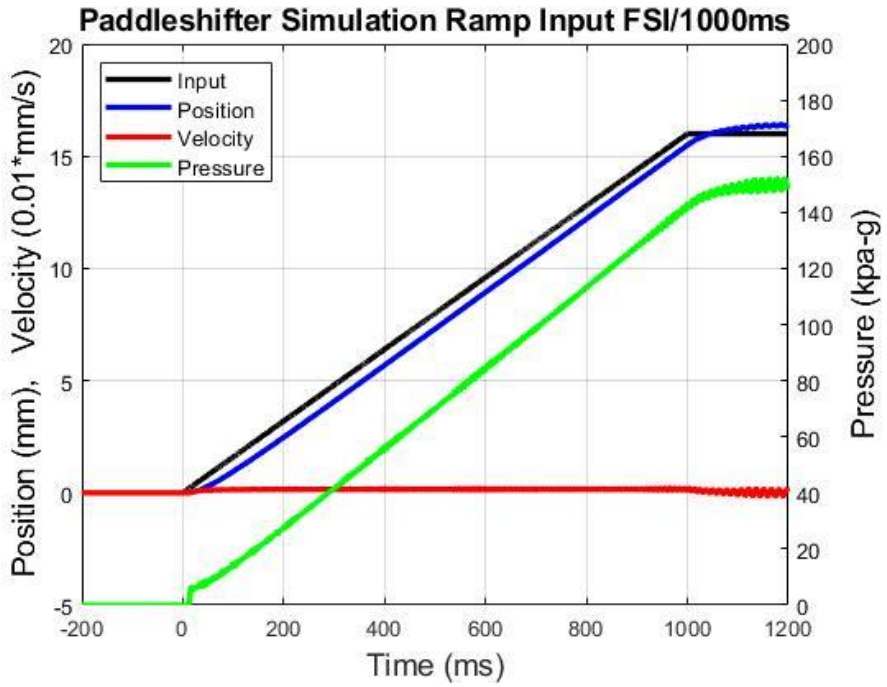

Fig. 2-17 Ramp-Step Response FSI/1000ms

If the simulation is run again for a slower input, this time a FSI/1s, the position lags the input by 39ms. This is shown in Fig. 2-17.

Running the simulation for a negative ramp-step input, i.e. starting at 16mm and ramping down to 0mm, yields a less stable- but still acceptable- response. This is shown in Fig. 2-18. The flow exiting the downstream fuel injector is not choked and will vary based on the pressure ratio across it. Thus, the velocity reduces as the position reduces, and the performance reaching 0mm is slower than a positive ramp input. The negative FSI/500ms ramp response lags the input by about 50ms with the performance decreasing as the actuator approaches 0mm.

One would think that reducing the cylinder area would help alleviate differences between positive and negative ramps. A smaller cylinder would require higher pressures. Higher pressures would cause the downstream injector to be choked more often, or at least be closer to choking. Surprisingly, reducing the area by roughly half, from 386mm^2 to 201mm^2, has a small effect on the downstream performance, as can be observed in Fig. 2-

19. Response lag is reduced to 40ms, but the performance as the position approaches 0mm is unchanged. Positive ramp performance is identical for the smaller cylinder size.

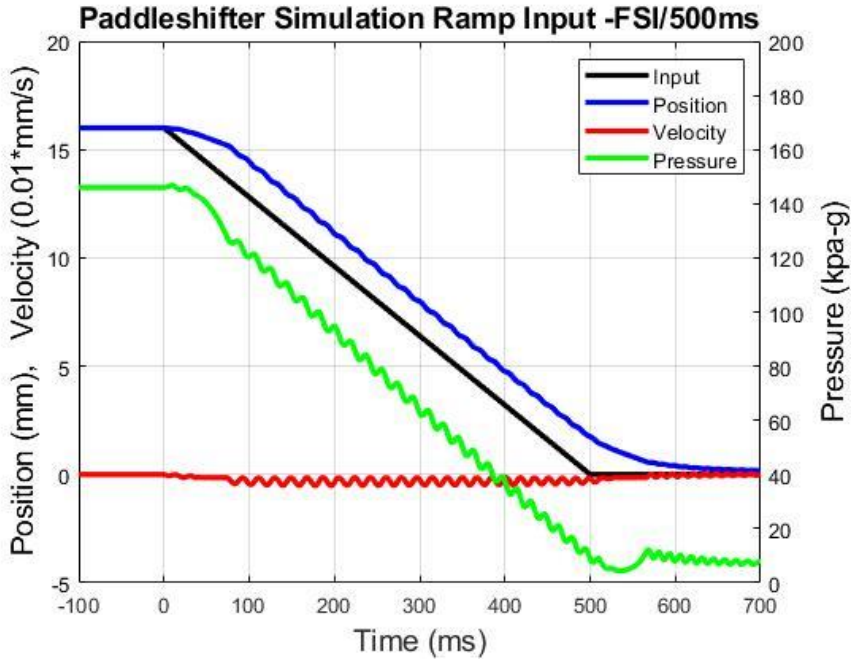

Fig. 2-18 Negative Ramp-Step Response FSI/500ms

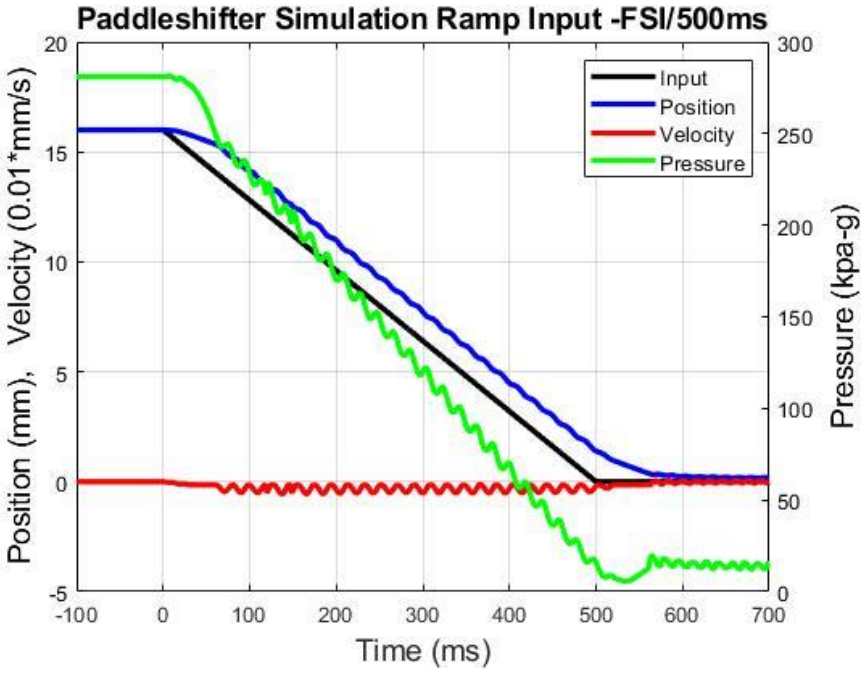

Fig. 2-19 Negative Ramp-Step Response FSI/500ms, Cylinder Area Halved

2.5.2 Step Input Response

A simulation of the 16mm FSI step input response is shown in Fig. 2-20. It settles in 250ms. Performance is limited by the filtering poles on the derivative gain. If these are all set to 630Hz, as opposed to 63Hz, the rise time is nearly cut in half, as shown in Fig. 2-21.

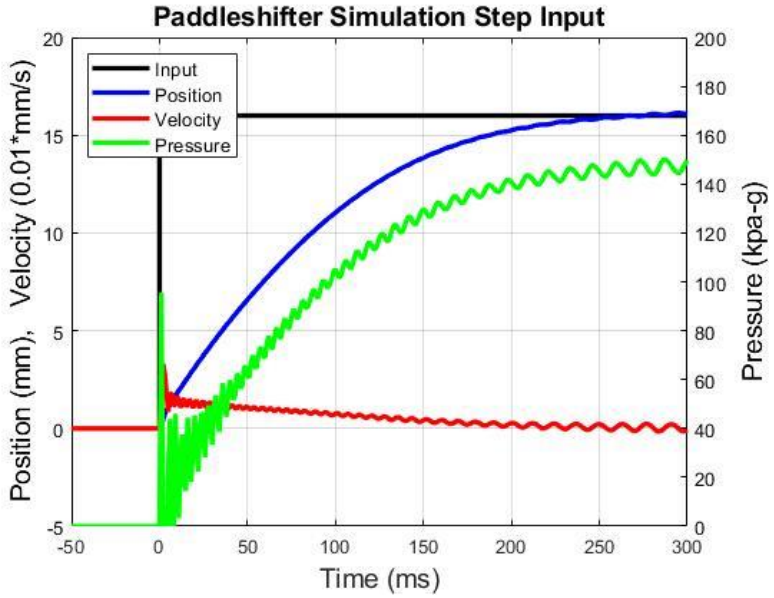

Fig. 2-20 Step Response

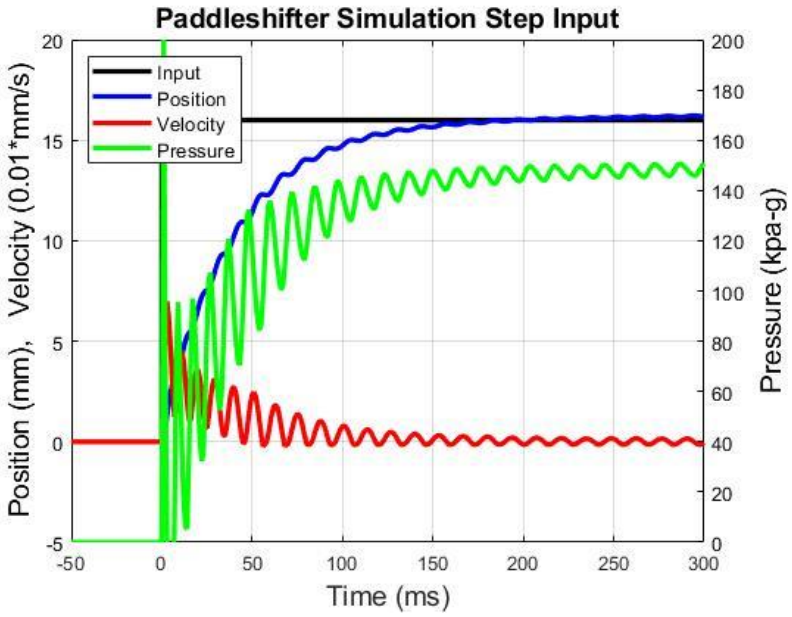

Fig. 2-21 Step Response with Derivative Gain Filters set at 630Hz.

While a filter frequency of 630Hz isn't realistic because it would attenuate too much electrical noise, this is an important observation. Following some real-world experimentation and some noise analysis, it may be possible to raise the filter frequencies and improve performance.

The response for a negative step input is shown in Fig. 2-22, the settling time is 130ms. The response is predominately overdamped with a few minor oscillations and slows considerably as the position approaches zero for identical reasons mentioned in reference to Fig. 2-18.

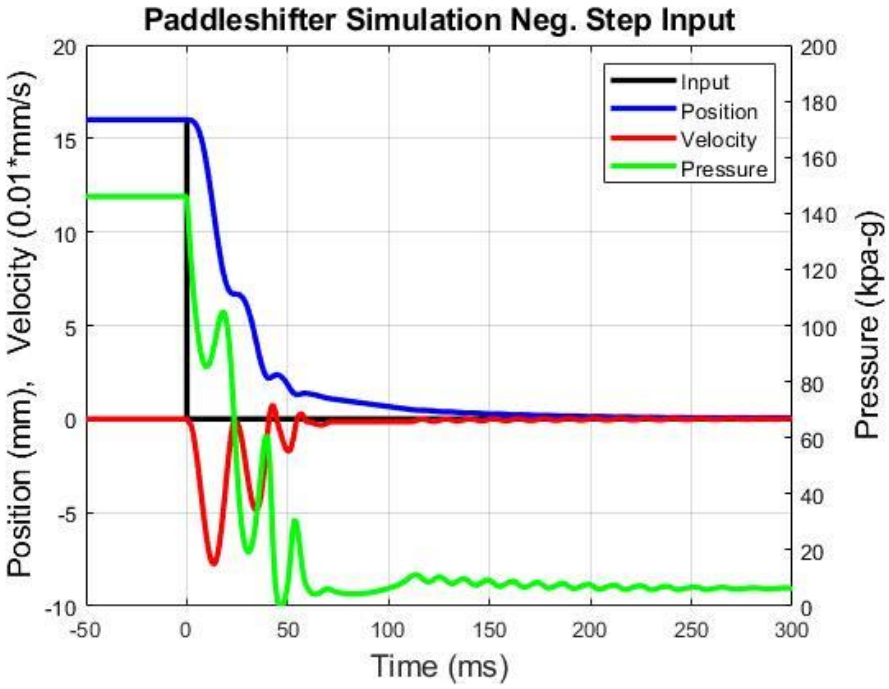

Fig. 2-22 Negative Step Response

2.6 Conclusions from Simulation

Obviously, reducing the capacitive volume between the injectors and the cylinder is a marked improvement. The injector block is mounted directly to the cylinder, joined by a 90° NPT fitting, to minimize this volume as much as possible. This configuration is shown in Fig. 2-23.

Fig. 2-23 Injector Block Mounted to Cylinder

Surprisingly, the system is not very sensitive to cylinder size. Air consumption does not change, as the same amount of energy is consumed with one actuation of the clutch. The main considerations for cylinder size are availability, packaging constraints, and weight.

The injectors are slightly too big. Currently, the injectors are rarely driven above a 70% duty cycle. The benefit of using a smaller injector would be its smaller minimum mass flow. CNG injectors, however, are not as prevalent compared to gasoline injectors and an "optimal" candidate is hard to find. Using a differently sized injector will require a new set of simulations and may require an integral gain if the injector is much smaller.

2.7 Weight Comparison

Weight is an obvious concern on a racecar. Components from both the mechanical shifter and pneumatic shifter were weighed and their summary is shown in Fig. 2-24. It is estimated the pneumatic shifter with the servo clutch will weigh approximately 2 pounds more than the mechanical shifter.

Mechanical Shifter		
Shifter	1.060	pounds
Linkages & Bellcranks	1.695	pounds
Clutch Cable	0.110	pounds
Total	2.865	pounds

Pneumatic Shifter			
Paintball Tank (Full)	3.250	pounds	
Shift Cylinder	0.365	pounds	
Clutch Cylinder & Injector Assembly	0.830	pounds	
Controller & Air lines	0.300	pounds	(est.)
Shift Valve	0.190	pounds	
Total	4.935	pounds	

Fig. 2-24 Weight Comparison between Mechanical Shifter and Pneumatic Shifter

It should be noted, however, that over 60% of the weight for the pneumatic shifter comes from the paintball tank. The tank which has been used thus far is a 68 ci tank filled to 4500 psi. Based on experience from testing, the current capacity is enough to comfortably last more than two FSAE or SCCA competitions. A tank of half the size is projected to weigh approximately 1.9 pounds, bringing the total weight to 3.6 pounds. While a larger tank is useful for a prototype configuration, a competition-ready solution should source a smaller air tank.

Chapter 3: Design

Most engineering research focuses heavily on analysis and theoretical design. The reality of building systems for an FSAE car is that they must actually be made and made to work reliably. Fortunately, this is representative of realistic design. This chapter discusses the various components which were built for the paddle-shifter system to operate. Physical or mechanical design is relatively simple and thus omitted in favor of electrical design aspects.

3.1 Gear Position Sensor

A gear position sensor, while not strictly necessary, will improve the reliability of the shifter actuation. Without it, the shifter cylinder and valve are operated in an open loop configuration, and mis-shifts sometimes happen. There are many variables, after all, involved in removing load from the engine just long enough to unload the transmission, and not too long to force engine braking to reload it, all synchronized to the actuation of a pneumatic cylinder. A closed loop system allows the controller to reliably actuate into the requested gear every time and provides a convenient method of actuating into the neutral gear.

The Yamaha R3 engine has a gear position sensor from the factory. It uses a rotary switch on the inside of the engine connected directly to the shifter drum. The contacts are embedded in a plastic housing attached externally. Each contact will switch to ground when in its corresponding gear, else the contact is floating.

As is, this system could be wired directly to seven microcontroller pins (Six gear positions plus one neutral position) with corresponding pull-up resistors. It is much more convenient, however, to use a single analog input pin instead. This requires running fewer wires and using fewer pins on the microcontroller.

This rotary switch can be rewired with resistors using the schematic shown in Fig. 3-1. A diode is added to the neutral contact to supply a ground path for the neutral light on the dash of the car.

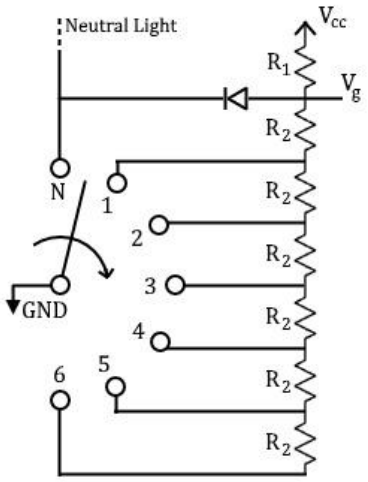

Fig. 3-1 Gear Position Sensor Wiring

The issue with using a voltage divider in this configuration is its non-linearity. The output voltage begins to saturate to the supply voltage at higher gears. See Fig. 3-2 and equation 3.1.

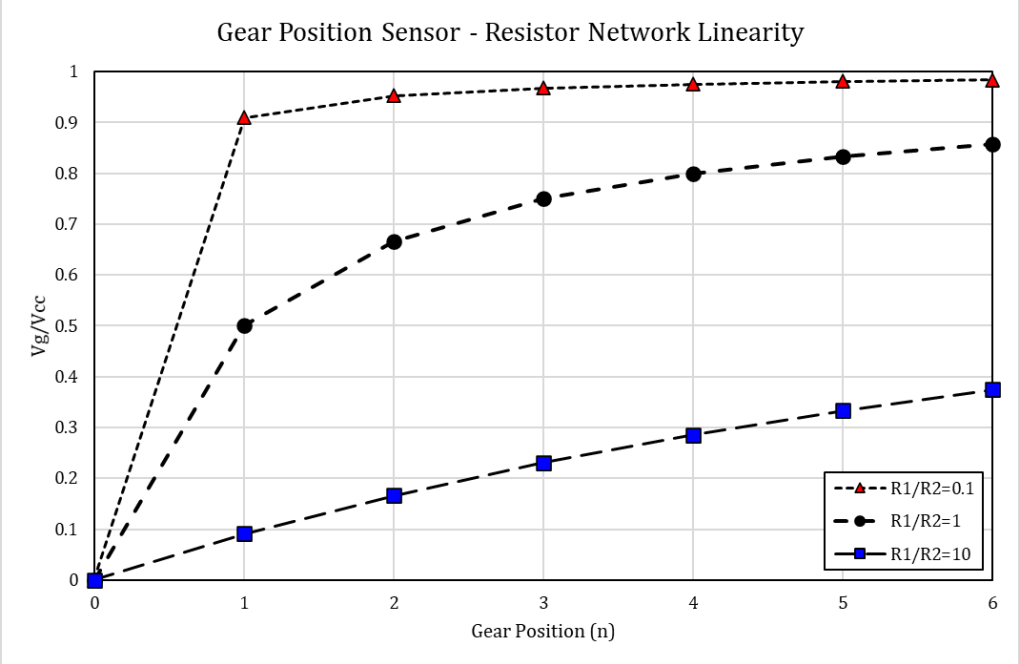

Fig. 3-2 Gear Position Resistor Network Linearity

$$V_{gear} = V_{cc} * \frac{n_{gear}R_2}{R_1 + n_{gear}R_2} = \frac{V_{cc}}{\frac{R_1}{n_{gear}R_2} + 1} \tag{3.1}$$

The microcontroller's ADC works from a 0-5V range, so the switch can be configured such that the largest output voltage is approximately 4V. By doing this and using a 12V supply rail, this arranges all of the signals into a relatively linear portion of this curve. This switch is a break-before-make switch, so the analog output will momentarily read 12V between gears. To the microcontroller's ADC, this will simply be perceived as 5V. Fig. 3-3 shows the input-output table for this configuration.

Vcc(V)	14.4
R1(kΩ)	150
R2(kΩ)	10

Gear:	Vg(V)
0	0.00
1	0.90
2	1.69
3	2.40
4	3.03
5	3.60
6	4.11
NC	14.40

Fig. 3-3 Gear Position Analog Sensor Output

The stock Yamaha sensor is potted with epoxy which must be removed. The majority of this epoxy and wiring is machined away, exposing each contact. Then the resistors are soldered as illustrated by Fig. 3-1, plus three wires and a diode. The sensor was re-potted with epoxy and re-installed, as shown in Fig. 3-4.

Fig. 3-4 Gear Position Sensor after machining (left), modified (center), installed (right)

3.2 Boost Converter and Constant Current Regulator

By applying higher voltages to an ordinary fuel injector, the current required to open the injector can be applied faster. Unfortunately, most fuel injectors will quickly

overheat if much more than 12V is applied to them. It is therefore necessary to utilize a constant current regulator in conjunction with the boosted voltage.

Note that utilizing a higher voltage and then a constant current source in series with the load decreases electrical efficiency. A more efficient method would be to dynamically adjust the voltage from a boost converter to provide effectively constant current. This avoids the additional energy dissipation of a series constant current regulator. Designing such a system is beyond the scope of this thesis, and the aforementioned simpler arrangement will be used.

In section 2.3 of this report, it has been shown why a 36V supply will be desirable. Such supplies are readily available in inexpensive boost converter configurations online, one of which is shown in Fig. 3-5.

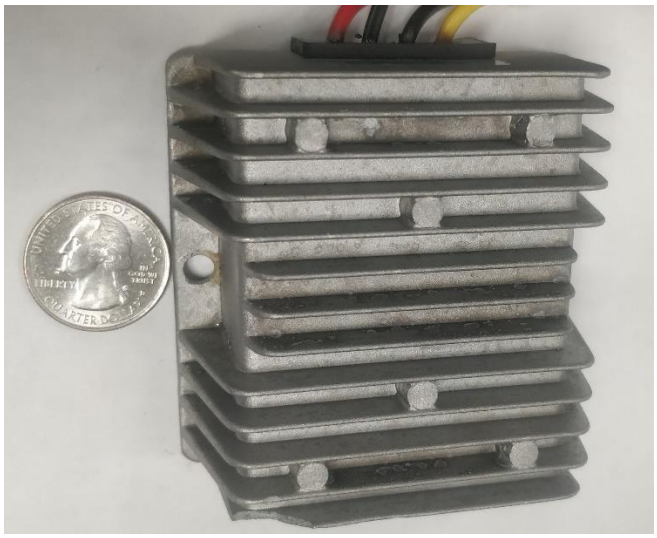

Fig. 3-5 36V Supply

A constant current source is most easily accomplished using a transistor. In this case, it is desirable to accomplish this regulation entirely from the positive rail of the boost converter, thus a PNP transistor is needed. This PNP transistor is provided a base current path through a Zener diode connected to the positive supply rail, an adjustable resistance, and an additional transistor which will fully conduct when a signal is perceived. The adjustable resistance sets the current limit. This circuit, along with a load which depicts the injector, is shown in Fig. 3-6.

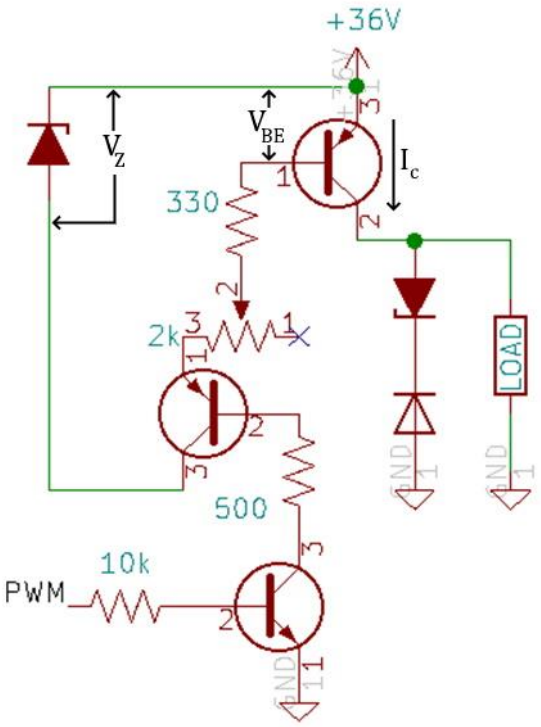

Fig. 3-6 Basic constant current source circuit

When 5V is applied to the PWM node of Fig. 3-6, the current is represented by equation 3.2.

$$I_C = \beta R_B (V_Z - V_{BE}) \tag{3.2}$$

As shown in Fig. 3-7, several transistors are attached in parallel with accompanying emitter resistors to share the current. These additional transistors are likely not necessary during normal operation; however, it is desirable to have extra thermal capacity to avoid any overheating issues during testing or driver-training where the clutch is actuated frequently. When the transistors are conducting, up to 40W could be expelled as heat.

The emitter resistors function to provide negative feedback for each transistor, ensuring each will be held at roughly equivalent currents. These are necessary due to transistors inherent thermal runaway properties. Additionally, the transistors are connected to a common heat sink so they will all be about the same temperature.

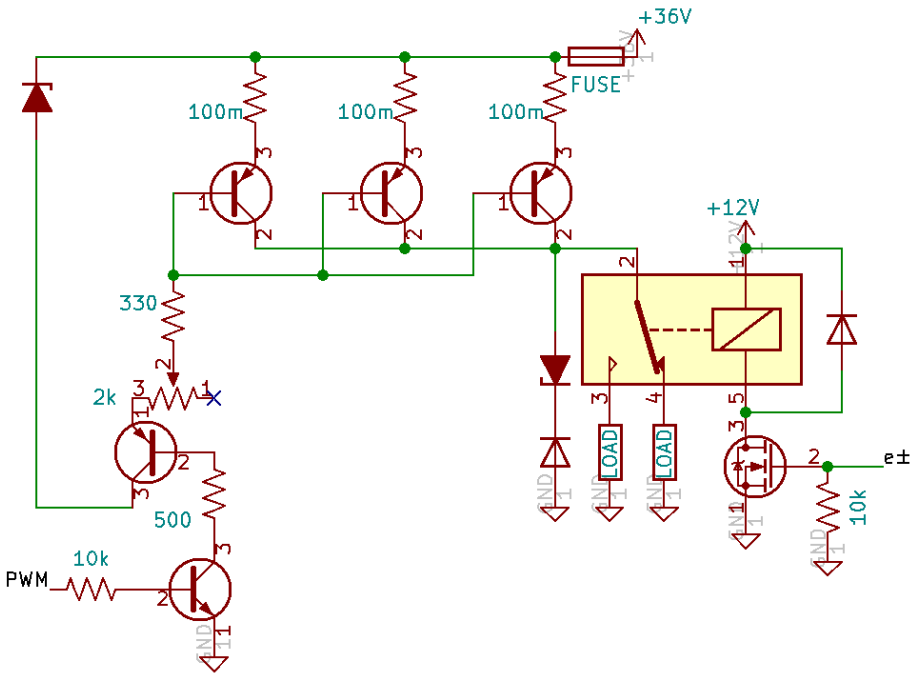

Fig. 3-7 Constant current source circuit with multiple transistors and injector selection

The load will need to be switched between the upstream and downstream injectors, thus a simple relay and supporting components were added following the main transistors. The switching delay of the mechanical relay is about 5ms. Such a delay is acceptable for selecting which injector to actuate because the system is predominately overdamped and will not be changing directions rapidly.

3.3 Controller Design

The paddle-shifter controller is configured as a half analog and half digital circuit. The pneumatic clutch feedback loop is controlled using analog circuitry mainly consisting of operational amplifiers. The shifter logic and launch control is operated digitally using a commercially available microcontroller, an Arduino Nano.

3.3.1 Analog Circuits

From a global perspective, the clutch circuit has two inputs, one from the command position, and one from the actuator position, and two outputs. In this case, the two outputs

are a PWM signal, whose duty cycle relates to the error of the system, and a binary output for solenoid selection. Positive and negative error both increase the PWM duty cycle, but the additional pin will switch to select which solenoid to actuate. By choosing this output format, it provides an opportunity for less components and a simpler circuit.

Fig. 3-8 is a block diagram of the circuit. The circuit has adjustable input/feedback gain, for the case where the full range of the input or position sensors cannot or should not be used. It also has adjustable proportional and derivative gain and deadband adjustment.

This design is not very hardware efficient. It uses a total of nine op-amps and could easily be reconstructed to use four or five. However, this configuration has the advantage of isolated adjustments: condensing the circuit usually means that adjustments will change multiple parameters, in this one, each parameter is adjusted individually. Following adjustment and testing, if this design is acceptable, a new design could be constructed which would be much smaller and cost effective.

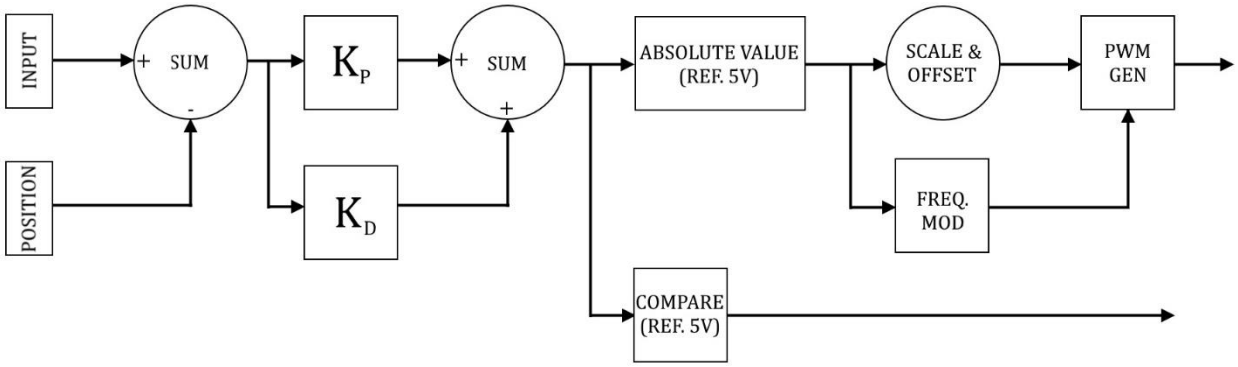

Fig. 3-8 Analog Circuit Block Diagram

There is a magnet embedded inside the piston of the actuator. This magnet is detected by an analog position sensor by SMC (PN# D-MP025C) and provides the position input. It outputs a voltage 0-10V over a 0-25mm range. This signal will go through a scaling circuit to define the maximum amount of travel intended for the application. The gain of this scaling will vary depending on the engine. A variable range of 0-12mm to 0-25mm is desired, which equates to a gain of 0.4 to 1.05. A small amount of leeway was provided for the case of component mismatch. This gain is represented by G_{fb} in equation 3.5. The scaling is accomplished by the circuit shown in Fig. 3-9.

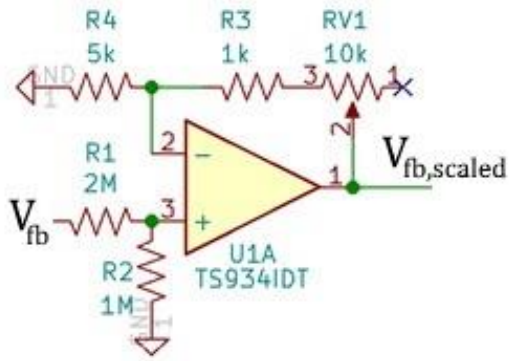

Fig. 3-9 Position Signal Scaling Circuit

The output from the circuit shown in Fig. 3-9 is defined by equations 3.3, 3.4, and 3.5. The variable RV_1 is used to represent a trimmer potentiometer which allows for the range adjustment. n_1 represents the adjustment of this potentiometer, ranging from 0 to 1.

$$V_{fb,scaled} = V_{fb}\left(\frac{R_2}{R_1 + R_2}\right)\left(1 + \frac{R_3 + n_1 RV_1}{R_4}\right) \tag{3.3}$$

$$V_{fb,scaled} = V_{fb} * \left(\frac{1}{3} + \frac{1 + 10 * n_1}{15}\right) \tag{3.4}$$

$$V_{fb,scaled} = V_{fb} * G_{fb} \tag{3.5}$$

The input potentiometer operates over a 10V-5V range. This arrangement allows a convenient method for achieving a 5V virtual ground. The summing circuit, shown in Fig. 3-10, subtracts the scaled position voltage from the input voltage. The controller's proportional and derivative gains will be adjusted later. Resistors R_1, R_2, R_5, and R_6 were specifically given high resistances to avoid their influence on the input sensors. The output of the op-amp is represented by equations 3.6, 3.7, and 3.8.

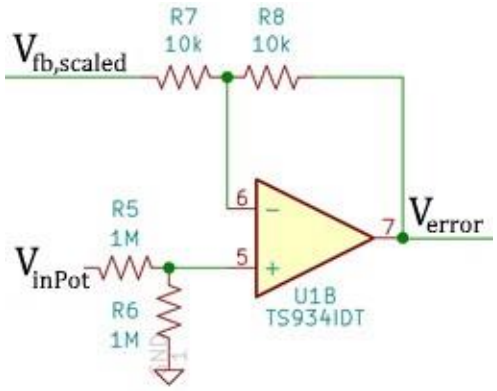

Fig. 3-10 Summing Circuit Detail

$$V_{error} = (V_{inPot} + 5V) * \left(\frac{R_6}{R_5 + R_6}\right)\left(1 + \frac{R_8}{R_7}\right) - V_{fb,sclaed} * \left(\frac{R_8}{R_7}\right) \tag{3.6}$$

$$V_{error} = (V_{inPot} + 5V) * 1 - V_{fb,sclaed} * 1 \tag{3.7}$$

$$V_{error} = V_{inPot} - V_{fb} * G_{fb} + 5V \tag{3.8}$$

The next part of the circuit converts the error into its proportional and derivative components, as well as allowing for adjustment of these gains and summing the components back together.

The proportional circuit is a low pass filter with an adjustable input resistance. The low pass filtering is present to remove any high frequency noise which may be present in the input signals. This filter is set to 10Hz. The variables RV_2 and n_2 represent the adjustment potentiometer which allows for fine tuning of the proportional gain. Using the arrangement depicted by Fig. 3-11, an adjustable proportional gain from 0.1 to 1.0 is achieved. This adjustment is based around the gain found from the simulation in section 2.5. The transfer function for the circuit shown in Fig. 3-11 is given by equations 3.9, 3.10, and 3.11.

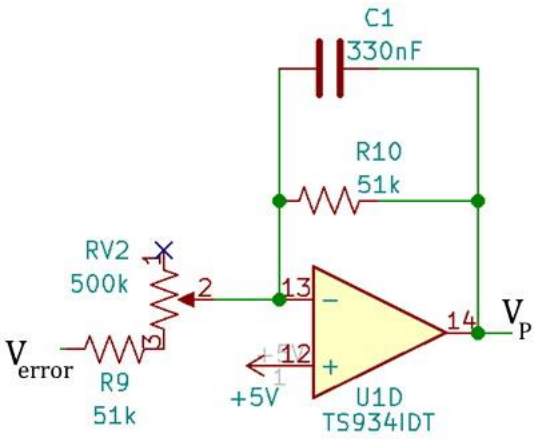

Fig. 3-11 Proportional Gain Detail

$$V_P = -V_{error} * \frac{R_{10}}{R_9 + n_2 * RV_2} * \frac{1}{(R_{10} * C_1)D + 1} \tag{3.9}$$

$$V_P = -V_{error} * \frac{51}{51 + n_2 * 500} * \frac{1}{\left(\frac{1}{60}\right)D + 1} \tag{3.10}$$

$$V_P = -V_{error} * \frac{K_P}{\left(\frac{1}{60}\right)D + 1} \tag{3.11}$$

The derivative circuit is based around two sallen-key low pass filters and a bandwidth-limited differentiator, shown in Fig. 3-12. The variables RV_3 and n_3 represent the adjustment potentiometer which allows for fine tuning of the derivative gain. The configuration shown in Fig. 3-12 allows for a derivative gain adjustment from 0.0125(12Hz) to 0.0625(2.5Hz). The transfer function for this circuit is given by equations 3.12, 3.13, and 3.14.

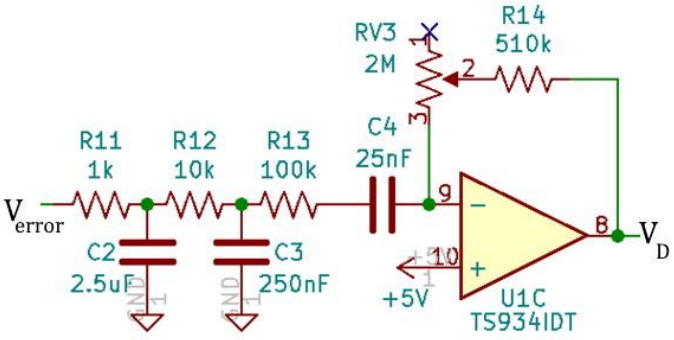

Fig. 3-12 Derivative Gain Detail

$$V_D = -V_{error} * \frac{1}{R_{11}C_2D + 1} * \frac{1}{R_{12}C_3D + 1} * \frac{(R_{14} + n_3RV_3)C_4D}{R_{13}C_4D + 1} \tag{3.12}$$

$$V_D = -V_{error} * \frac{1}{\left(\frac{1}{400}\right)D + 1} * \frac{1}{\left(\frac{1}{400}\right)D + 1} * \frac{.025(0.51 + 2 * n_3)D}{\left(\frac{1}{400}\right)D + 1} \tag{3.13}$$

$$V_D = -V_{error} * \frac{K_D D}{\left(\left(\frac{1}{400}\right)D + 1\right)^3} \tag{3.14}$$

Note that if the resistance of the two adjacent sallen-key filters are similar, the filter quality will greatly degrade. Ideally, a ratio of 100:1 or greater would be best, but in this case, a ratio of 10:1 must be used due to upper resistance limitations.

The proportional error voltage and derivative error voltage must now be summed together, this is accomplished using the circuit shown in Fig. 3-13. Assuming all resistances are equal, this circuit is represented by equation 3.15.

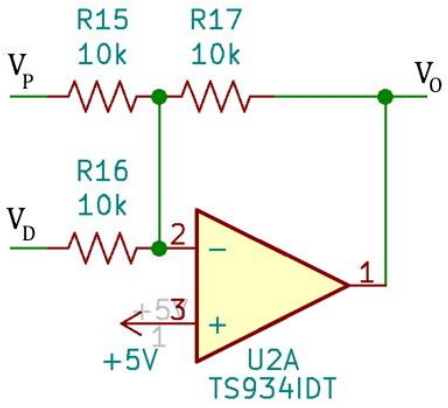

Fig. 3-13 Proportional and Derivative Error Summing Detail

$$V_o = -V_P - V_D \tag{3.15}$$

Once the command has been calculated from the error, the absolute value must be taken about +5V using the circuit shown by Fig. 3-14. If all of the resistors are of equivalent resistance, the output is given by equation 3.16.

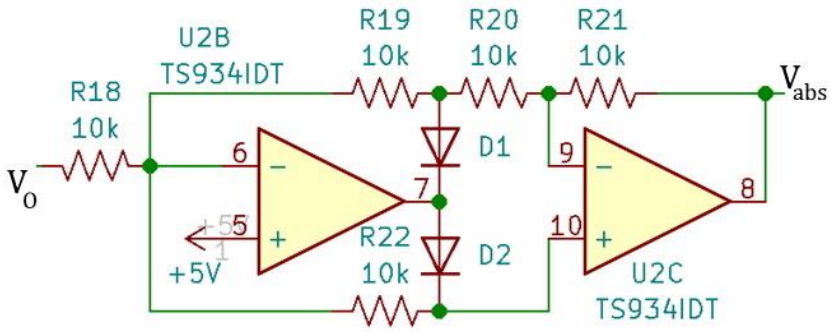

Fig. 3-14 Absolute Value Circuit Detail

$$V_{abs} = |V_o - 5V| + 5V \tag{3.16}$$

The next portion of the circuit scales and offsets the input. This is necessary for the PWM generator which follows. The PWM generator operates from a 100mV to 900mV input voltage range, with the voltage proportionally relating to the duty cycle. For this reason, it is necessary to scale and offset our input voltage from a 5V-10V range down to a 100mV-900mV range. A deadband adjustment can also be made by adjusting the offset to values lower than 100mV, where no PWM signal will be output. This deadband adjustment is represented by n_4 and RV_4. The PWM generator IC can accept input voltages up to its supply rail of +5V, thus the output does not need to be saturated, since the maximum input to this op-amp will be +10V, and the maximum output will then be below +5V. Voltages above 900mV will continue to output a 100% duty cycle.

The scaling circuit is shown in Fig. 3-15 and the output is given by equations 3.17, 3.18, and 3.19. This configuration allows for a minimum value adjustable between 50mV and 105mV. Note that by adjusting n_4, and thus adjusting the deadband, the gain of the controller also changes. It is intended that this variable will not be adjusted very frequently and will likely be set during initial setup without further changes. Assuming nominal device parameters [5], a maximum deadband of 8% of the full range of travel is possible.

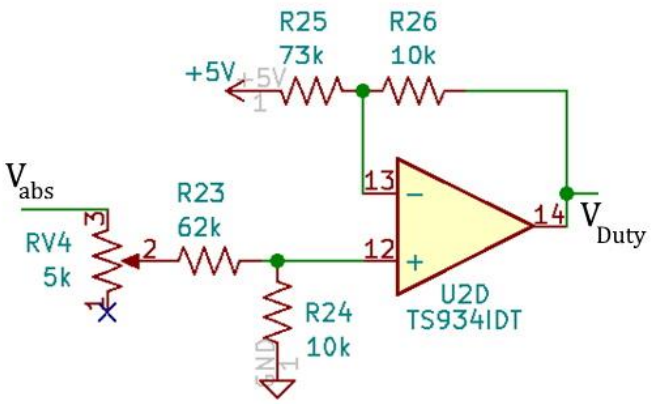

Fig. 3-15 Scale and Offset Circuit Detail

$$V_{Duty} = V_{abs} * \frac{R_{24}}{R_{23} + R_{24} + n_4 R V_4} * \left[1 + \frac{R_{26}}{R_{25}}\right] - 5V \left[\frac{R_{26}}{R_{25}}\right] \tag{3.17}$$

$$V_{Duty} = V_{abs} * \frac{10}{72 + 5 * n_4} * \left[1 + \frac{1}{7.3}\right] - 5V \left[\frac{1}{7.3}\right] \tag{3.18}$$

$$V_{Duty} = V_{abs} * \frac{11.37}{72 + 5n_4} - 0.685V \tag{3.19}$$

The next step in the circuit is the PWM generator. It is the LTC6992 IC by Analog Devices. This chip was used to simplify the circuit and reduce cost. It requires only a few external resistors to operate as necessary. Two resistors act as a voltage divider on pin 4 and select the coarse frequency range and gain polarity. The fine adjustment of frequency depends on the current draining from the constant 1V source on pin 3 to ground. The frequency is given by equation 3.20.

$$f = \frac{1MHz * 50k * I_3}{N_{div} * 1V} = 48.85 I_3 * 10^6 \tag{3.20}$$

According to the device datasheet [5], the set current should not be less than 1.25µA or greater than 20µA. A frequency of 60Hz requires a set current of 1.25µA. 500Hz requires 10µA. The frequency can be derived from the circuit shown in Fig. 3-16. The current draining from pin 3 is described by equation 3.21. For 0% duty cycle, equation 3.22 applies. For a $(V_f - V_{be})$ of 0.7 volts, equation 3.23 applies.

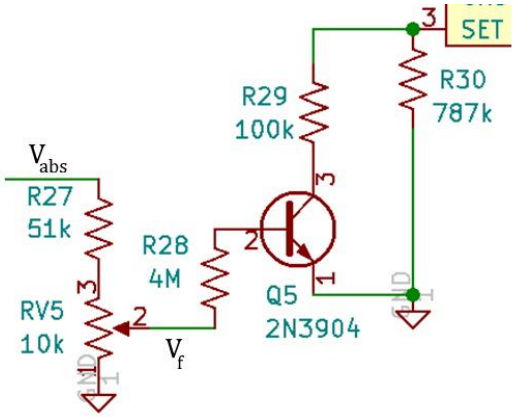

Fig. 3-16 Frequency modulation circuit

$$I_3 = \frac{1V}{R_{30}} + \left(V_f - V_{be}\right)\frac{h}{R_{28}}, \qquad while\ \left(V_f - V_{be}\right) < \frac{1V * R_{28}}{hR_{29}}\ and\ V_f > V_{be} \tag{3.21}$$

$$I_3 = \frac{1V}{R_{30}} = \frac{1V}{787k\Omega} = 1.27\mu A \tag{3.22}$$

$$I_3 = \frac{1V}{R_{30}} + \frac{0.7V * h}{R_{28}} = \frac{1V}{787k\Omega} + \frac{0.7V * 100}{4M\Omega} = 20\mu A \tag{3.23}$$

The purpose of R_{29} is to prevent damage to the chip by drawing too much current, so a value of 100kΩ can be used.

An input voltage range of 0.7V was used because this is a typical value for V_{be} as well. The output of the absolute value circuit, which outputs from 5V-10V, is scaled down using a simple voltage divider to 0.7V-1.4V. The upper frequency is less important than the lower frequency, thus a simple voltage divider can be used. The voltage divider shown in Fig. 3-16 is capable of adjusting the 5V minimum input anywhere from 0-0.8V.

The final part of this circuit is what selects which solenoid to actuate. It uses an op-amp to compare the error signal to a +5V reference. If it is higher, +10V is output. If it is lower, 0V is output. This circuit is shown in Fig. 3-17.

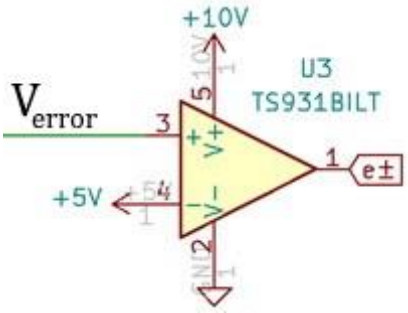

Fig. 3-17 Error Comparator Detail

3.3.2 Digital Circuits

The digital circuits consist of the shifter control, the ECU outputs, and the launch control. An Arduino Nano connects to three switches with internal pull-up resistors. One for upshifting, one for downshifting, and one for launch control. Inputs for the input command and clutch position are provided for later conditions concerning launch control.

The valves which switch the pneumatics are simple 350mW valves, and do not require a robust switching device. Thus, common 2N7000 MOSFETs were used in the configuration shown in Fig. 3-18.

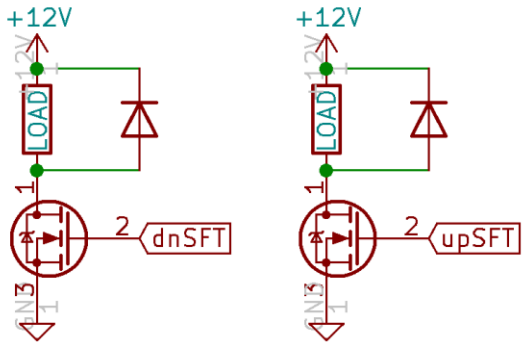

Fig. 3-18 Shifter MOSFET Configuration

Two outputs of the microcontroller are connected to the ECU. One commands the ECU to cut ignition for a set amount of time, and the other commands the ECU to apply a maximum RPM for as long as the pin is held at ground. The latter is used for launch control.

The former is used for shifts and simply shares a pin with the MOSFET gate which actuates the upshift valve.

The program required for shifting works from a request queue, similar to a FIFO buffer. The program counts how many times the buttons were pressed, then executes the commands when available. This is necessary because the cylinder requires some time to retract before the next shift is attempted.

Before the car is launched, but after launch control is engaged, the clutch position must be held at a point just before it engages. This helps get a repeatable result. During the launch, the clutch must be released at a specific, and tunable, rate. This rate, in addition to the holding RPM and starting manifold pressure, will dictate the amount of wheelspin during the launch.

To force the analog circuit to apply this clutch position and error rate, two SPDT analog switch IC were placed to override the circuit when necessary. The switches are controlled through the Arduino. To generate the analog signals which will be applied to these switches, the average voltage of a PWM signal is used, with the duty cycle adjustable in the microcontroller. MOSFETs are applied in the circuit such that a reference voltage switches between the maximum and minimum desired output voltage as the gate voltage is switched. A smoothing capacitor is added to average the signal.

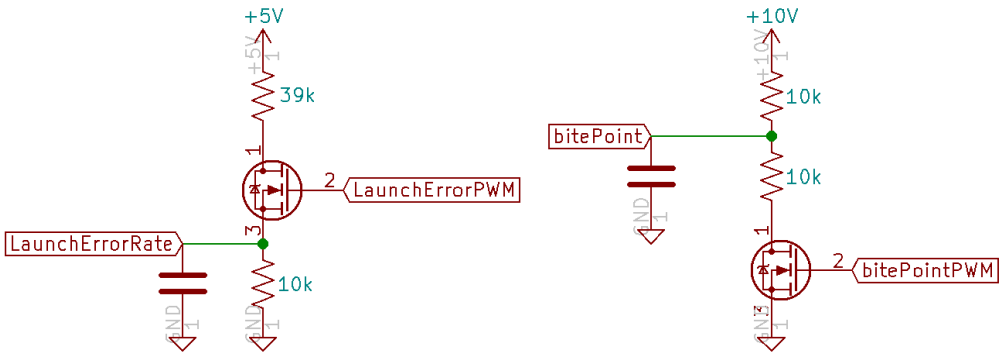

Fig. 3-19 Launch Control - Analog Outputs

3.4 Examining Controller Response

Following the construction of the printed circuit board the P and D parameters are tuned manually. This was completed by following the same procedure outlined in section 2.5. The proportional gain was adjusted to 0.75, and the derivative gain was adjusted to 0.038. These gains are extremely close to what was predicted from the simulation, which indicates a relatively high degree of simulation accuracy.

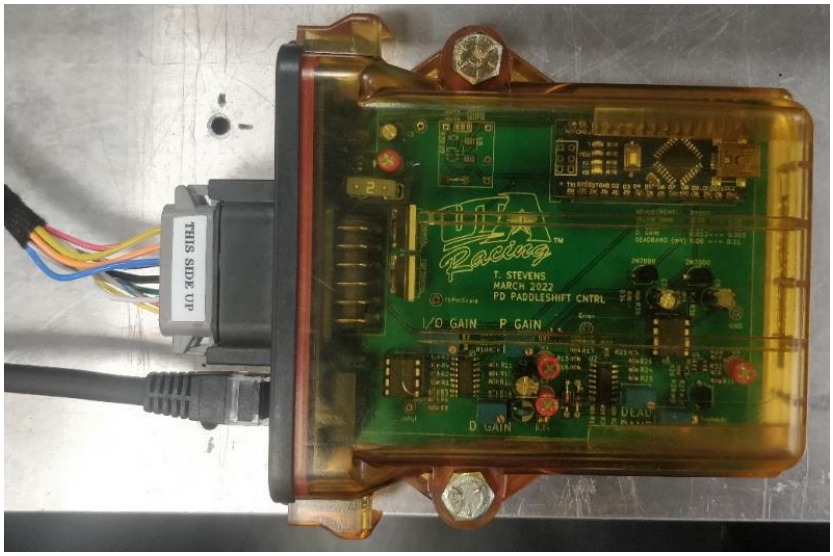

Fig. 3-20 Finished Controller PCB

The first data to collect to characterize the controller is a sudden step input, shown in Fig. 3-21. This will illustrate the controller delay, i.e., the time between an input and the controller's corresponding command. This delay will vary somewhat depending on when the step input is provided relative to the PWM cycle. This latency is measured by inspecting the input command and controller output signal and recorded to be less than 6ms. This data was collected using a RIGOL DS1054Z oscilloscope with 8 bits of vertical resolution.

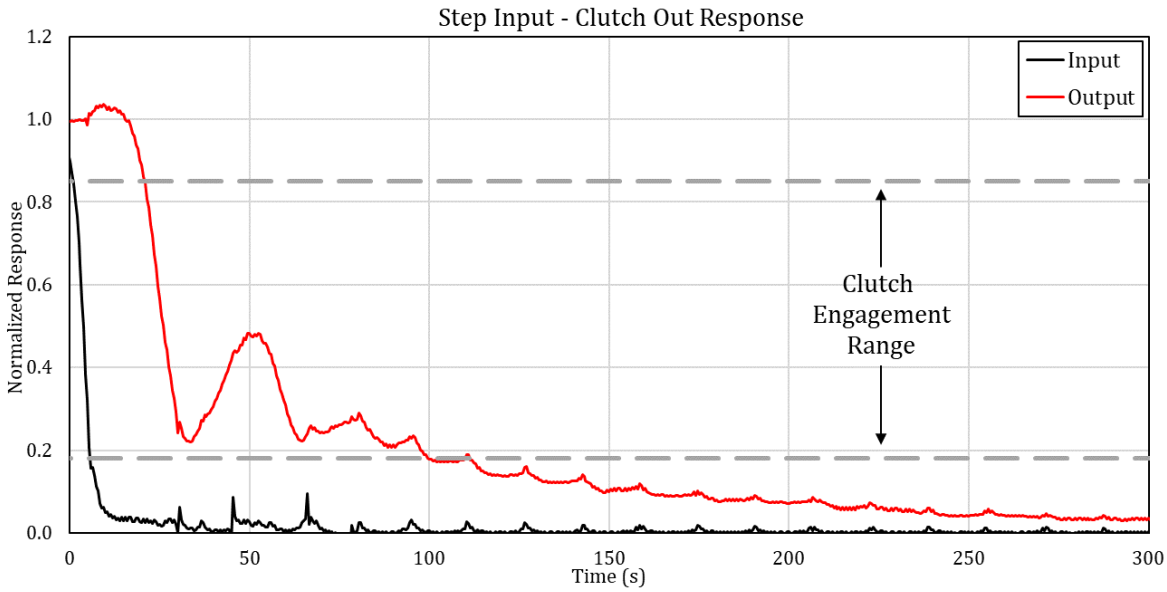

Fig. 3-21 Step Input - Clutch Release Experimental Response

The step input for releasing the clutch responds slower than the simulation, settling approximately 100ms later than predicted. I believe this is because of how the clutch springs engage inside the engine. Once the clutch is fully engaged, the force from the clutch springs abruptly stops. Since this is the main extension force, when it ceases, the response slows. This is acceptable however, because once the clutch is fully engaged, the remaining travel is not important.

Another behavior to note is the oscillation at 50ms. This is caused by the filtering latency in the derivative gain circuit causing the controller to momentarily engage the upstream injector. Unfortunately, the filtering must remain to avoid electrical noise on the derivative circuit, however, this oscillation can remain with no consequences. This oscillation only occurs with a step input, which is impossible when using the steering wheel inputs as designed. The clutch paddle attached to the input potentiometer has its own spring and mass which prevents step releases. Furthermore, an oscillation over such a small period of time will not affect the performance of the system in practice.

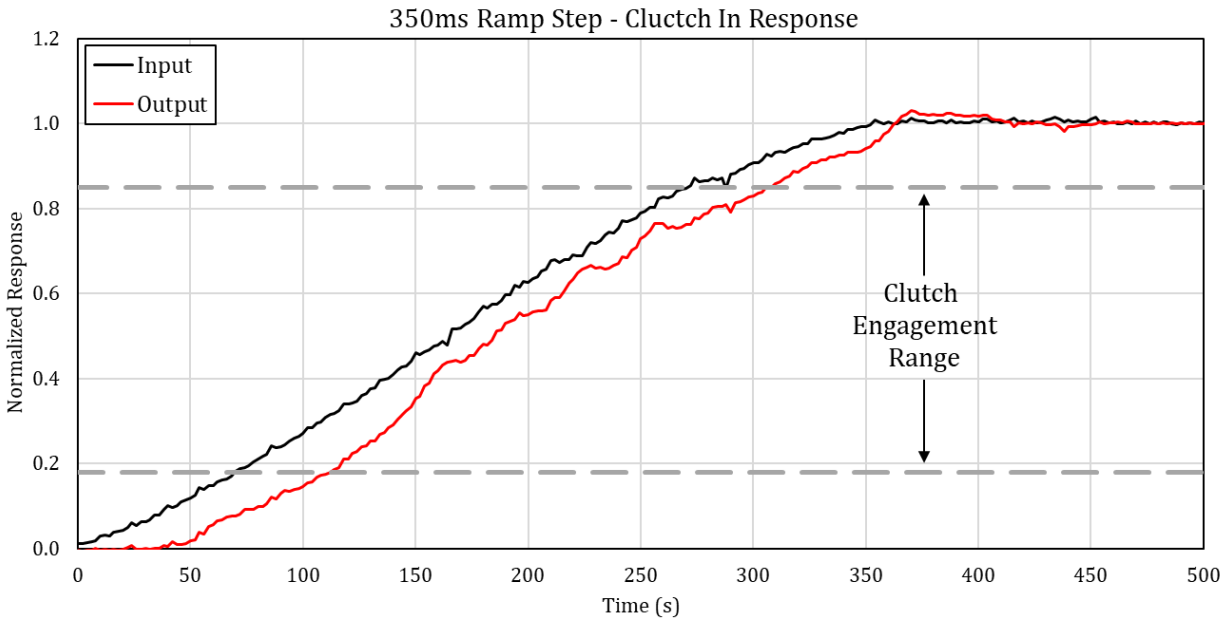

Fig. 3-22 350ms Ramp Step – Clutch in Experimental Response

A ramp-step input of 350ms is shown in Fig. 3-22. The position lags the command by approximately 30ms and shows behavior similar to the MATLAB simulation. Being experimental data, there are a few minor oscillations, but otherwise the response provides smooth clutch operation.

Chapter 4: Conclusions

In this document, I have covered the analysis conducted to refine system parameters, starting with the characterization and accurate simulation of the CNG fuel injectors, as well as the modeling of the pneumatic actuator dynamics. It was found that using a higher supply voltage in conjunction with a constant current limiter to drive the injectors allowed for increased performance by way of a smaller deadband and more linear behavior. A PD controller was selected and tuned using this simulation. The electrical circuits required for an analog PD controller were derived and explained. A printed circuit board was constructed and tested based on these circuits. The servo clutch provides stable and predictable performance. Experimental data shows that the clutch position lags the input command by less than 50ms during a typical clutch release. This provides a successful method of operating the clutch precisely.

The pneumatic shifting system allows for consistent 50ms long shifts. The mechanical system shifts in 200ms on average. The reduced shift time of approximately 150ms adds up quickly in a competition where every tenth of a second is important. The advantages for the driver, i.e., shift consistency and reduced distraction, is likely to make a positive impact on performance as well. This shifter system also alleviates the need for mechanical linkage which is often difficult to package. The pneumatic shifting system offers more consistent and higher performing shifting than the mechanical system.

The 2018 and 2022 UTA Formula SAE cars are configured for the electro-pneumatic shifter and servo clutch system. The electro-pneumatic system can easily be adapted to different engines. Ideally, a new simulation would be executed to ensure its performance, however, this may not be strictly necessary due to the relatively high actuator force potential and responsiveness. The simulation variables which will change from engine to engine would largely be overshadowed by the power of the actuator.

This thesis delivers a complete paddle-shifter system in an industry-level package which can easily be installed without detailed knowledge of its design. The performance of the system has been carefully refined to be as responsive as possible while maintaining

stability. The paddle-shifter system has been tested extensively to prove its reliability in comparison to a mechanical alternative.

Future work on this controller may entail the integration of an electronic throttle. The main benefit being a more sophisticated closed loop launch control system, however this would also allow for smoother and possibly faster shift times.

Appendix A: Coulomb Force Model

This is a brief summary of the Coulomb Force Model described in Dr. Woods' Paper *Coulomb Friction Between Two Moving Bodies Including Static and Dynamic Motion* [9].

There are three states to consider:

- Body In Motion: Where the velocity is nonzero and frictional force is a constant value.
- Captured and Static: Where the velocity is zero and the sum of the forces applied to the body (excluding frictional force) is overcome by coulomb friction.
- Captured but Accelerating: Where the velocity is zero, but the sum of the forces applied to the body (excluding frictional force) is not overcome by coulomb friction.

Velocity in a digital simulation will never be equal to zero, thus zero velocity is defined as being less than V_{min}, shown by equation A.1. V_{min} is defined based on the acceleration from coulomb friction making the velocity go to "zero" in one time step.

$$when \;\; |V| \leq V_{min}, \qquad where \;\; V_{min} = \frac{f_c \Delta t}{M} \tag{A.1}$$

The above conditions are rewritten in equations A.2, A.3, and A.4. $F_f(\dot{z})$ is the output frictional force.

$$if \; \Sigma F < f_c \; \& \; |V| \leq V_{min}, \qquad then \; F_f(\dot{z}) = \Sigma F \tag{A.2}$$

$$if \; \Sigma F \geq f_c \; \& \; |V| \leq V_{min}, \qquad then \; F_f(\dot{z}) = f_c * sign(\Sigma F) \tag{A.3}$$

$$if \; |V| > V_{min}, \qquad then \; F_f(\dot{z}) = f_c * sign(V) \tag{A.4}$$

f_c represents the coulomb friction saturation value.

Appendix B: Experimental Data Collection for Injector Model

This appendix describes the process used to characterize the electromagnetic force generated by a fuel injector using experimentally collected data. First, a solenoid is used to describe the force vs. displacement and force vs. current relationships. Secondly, a fuel injector is evaluated to develop a generalized model.

Solenoid Test Setup

The solenoid which will be tested is a Camozzi A72 with a resistance of 30Ω, which has been modified to accept a nylon screw which passes through the solenoid, connecting to the ferrous shuttle. The original solenoid also had a preloaded spring, which has been removed. The solenoid is placed onto an aluminum block, which is drilled to allow the shuttle to extend below the solenoid body, shown in Fig. B-1.

Fig. B-1 Assembled Solenoid and Base(left), Shuttle with added Nylon Screw(right)

These parts were placed onto an IMADA ZTA-11 digital force gauge, which measures force and vertical displacement, and allows for precise control of shuttle displacement. The solenoid was wired to a power supply providing a constant current. This test setup is shown in Fig. B-2.

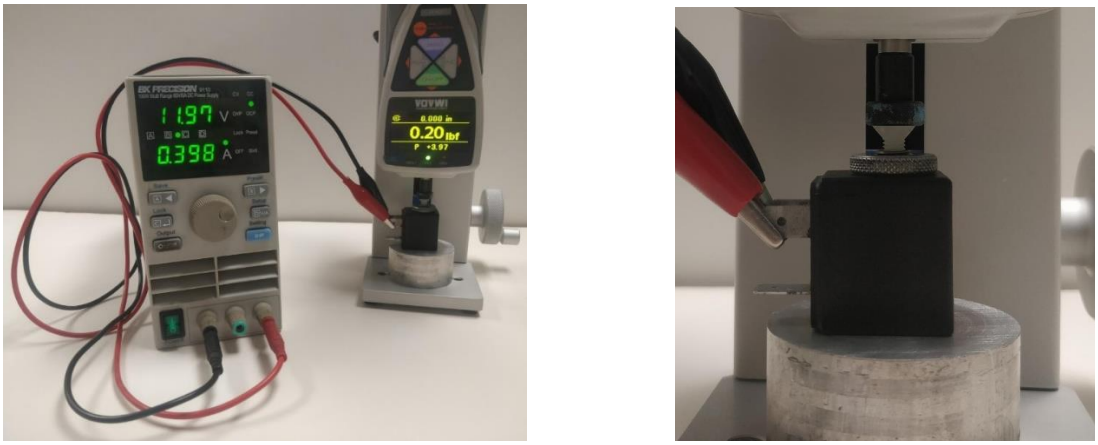

Fig. B-2 Solenoid Test Setup(left), Close-up View(right)

Solenoid Force vs. Displacement Characteristic

Using the IMADA software, the force and displacement of the shuttle was recorded with a constant current of 400mA, shown in Fig. B-3. The data has been offset such that zero displacement is when the shuttle bottoms out in the solenoid.

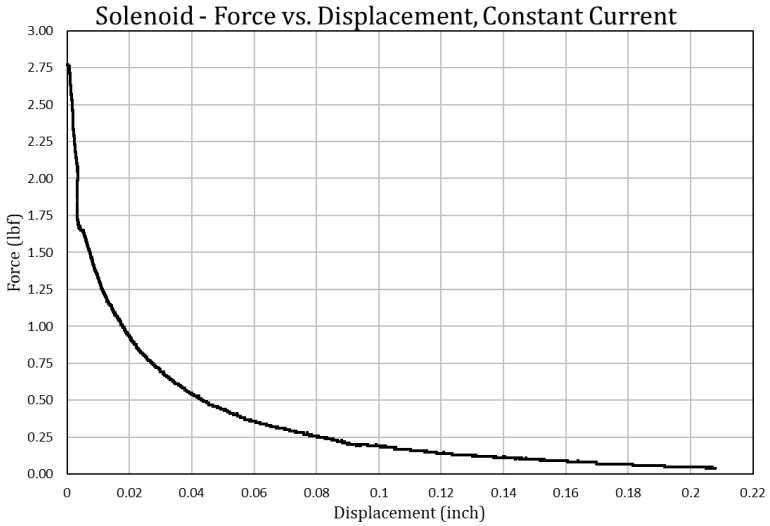

Fig. B-3 Experimental Force vs. Displacement Characteristic Curve

As expected, the electromagnetic force is wildly nonlinear with respect to position. Luckily, considering the relatively small range which a fuel injector's shuttle moves, linearization will likely be a suitable approximation.

Solenoid Force vs. Current Characteristic

To determine the force vs. current characteristic, the force gauge was lowered 0.030". This height will provide a good compromise between force sensitivity to vertical height and producing a larger signal to provide more resolution from the gauge.

In 50mA increments, the current was increased, and the force was recorded. This is shown in Fig. B-4. Special care was taken to avoid the coil getting too hot, with occasional breaks to allow the solenoid to return to room temperature.

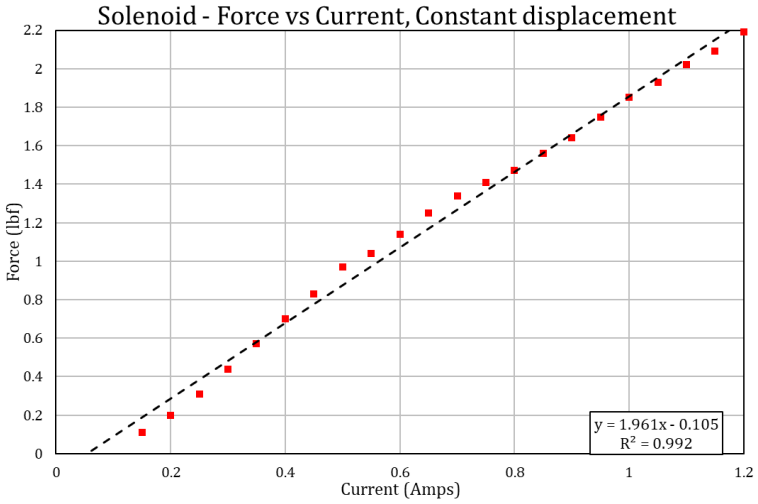

Fig. B-4 Experimental Force vs. Current Characteristic Curve

Following with theory, this data suggests a linear relationship. Of course, once the coil begins to saturate, the gain will decrease and approach zero. Power supply limitations and heat generation concerns prevented measuring coil saturation behavior.

Injector Test Setup

Similar to the solenoid tested previously, the injector which was evaluated was lightly modified. The injector's inlet strainer was removed which provides a direct path to the center of the shuttle. A piece of 0.08" aluminum rod was placed into the injector, allowing direct measurement of force and displacement. The injector is placed into a

machined piece of aluminum which ensures perpendicular alignment. These parts are shown in Fig. B-5.

Fig. B-5 Aluminum Base, Fuel Injector, and Aluminum Rod used for Fixturing

The modified injector was first placed below a depth indicator, so the precise stroke of the shuttle could be measured, shown in Fig. B-6. In this case, it is 0.003".

Fig. B-6 Measuring Injector Stroke

Force vs. Current and Position Characteristics of a Fuel Injector

The fuel injector assembly was placed in the same apparatus as before, allowing control of input current and position, while displaying the force, current, and displacement measurements. This is shown in Fig. B-7.

Fig. B-7 Injector Test Setup (left), Close-up view of Injector (right)

This data will be used to generate a linearized model for the electromagnetic force of the fuel injector. Multiple data points are desired, however given the small range of 0.003”, only a few position data points could be collected.

It was quickly discovered that the injector operated largely in saturation. Therefore, force was recorded up to 4.5A in 500mA steps, with extra data points recorded in the unsaturated regions. This process was conducted at X=0 (shuttle fully closed), at X=0.0013”, and X=0.0023”. As before, special care was taken to avoid overheating the injector and breaks were taken occasionally to allow the injector to cool to room temperature.

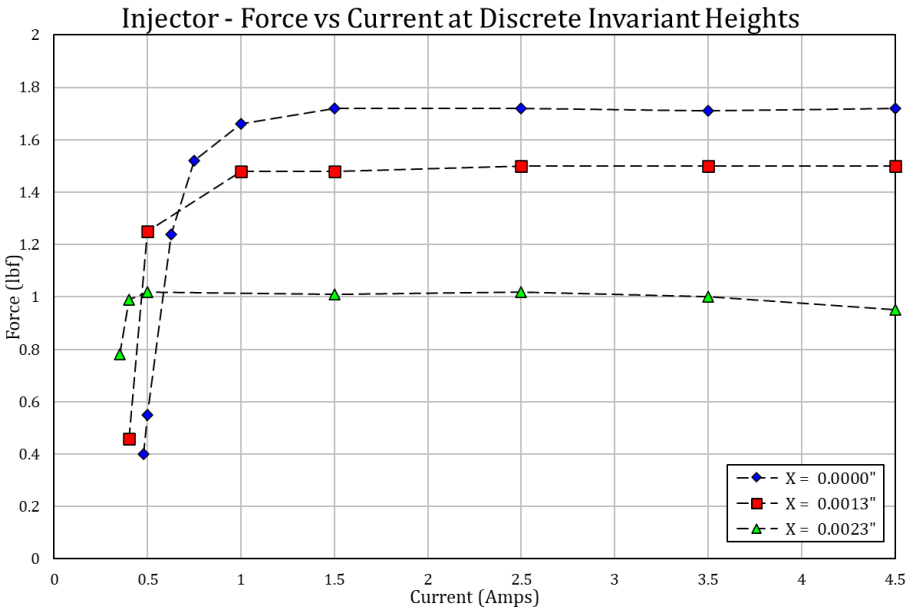

Fig. B-8 Experimental Force vs. Current and Displacement Data

The behavior shown in Fig. B-8 is exactly what I would expect from a fuel injector. The shuttle was situated such that the highest forces occur as the injector is opening, with lower forces present when the injector is completely open. This arrangement should allow for faster opening times, and thus smaller minimum duty cycles. This follows the same logic of a peak-and-hold pre-driver providing peak current as the injector opens and holding a lower current to keep it open.

A model is constructed from the acquired data with a linear unsaturated region and a variable saturation point, depending on the shuttle displacement. A positive force offset was applied such that no force is generated when current is equal to zero. This pre-existing offset exists because of the spring preload inside the fuel injector and was confirmed by measuring parts from a disassembled injector.

As was seen from testing the solenoid through a wide range of displacements, the force-displacement relationship is nonlinear. This linearized model is only applicable for the range of the fuel injector stroke.

The linear section is described by equation B.1, and the saturation force threshold is described by equation B.2. These equations are represented in Fig. B-9.

$$F_{EM} = 4.2\frac{lb_f}{A} * I_L, \qquad 4.2\frac{lb_f}{A} = 18.7\frac{N}{A} \tag{B.1}$$

$$F_{EM\_Sat} = -263.8\ \frac{lb_f}{inch} * x + 2.8\ lb_f, \quad 263.8\ \frac{lb_f}{inch} = 46.2\ \frac{N}{mm}, \quad 2.8\ lb_f = 12.5\ N \tag{B.2}$$

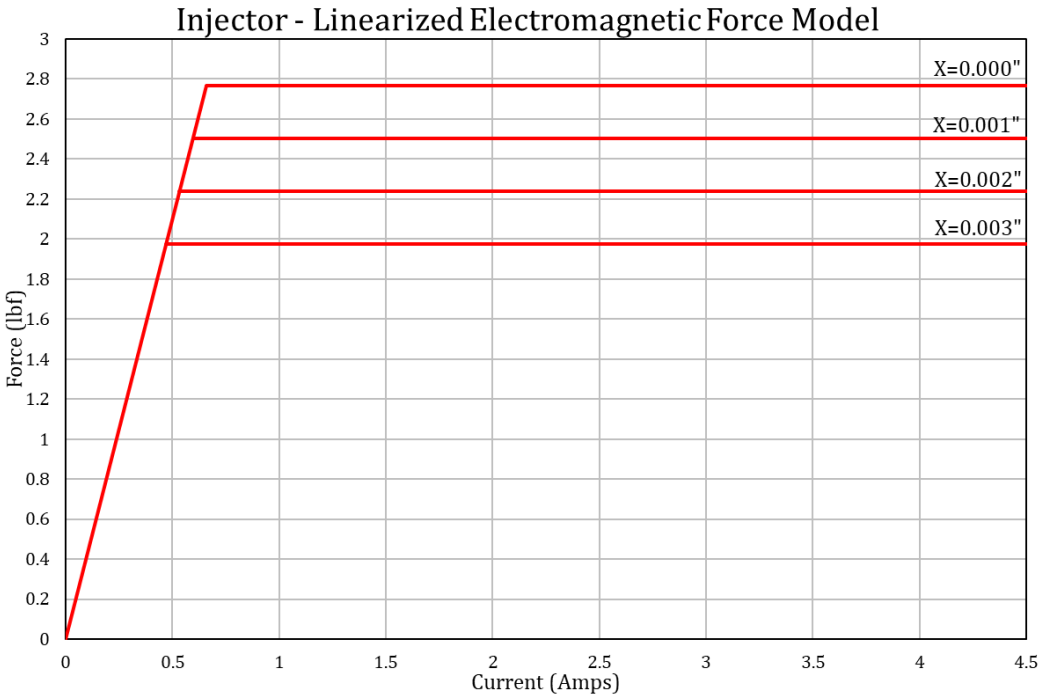

Fig. B-9 Linearized Electromagnetic Force Model

Appendix C: Analog Circuit Schematic

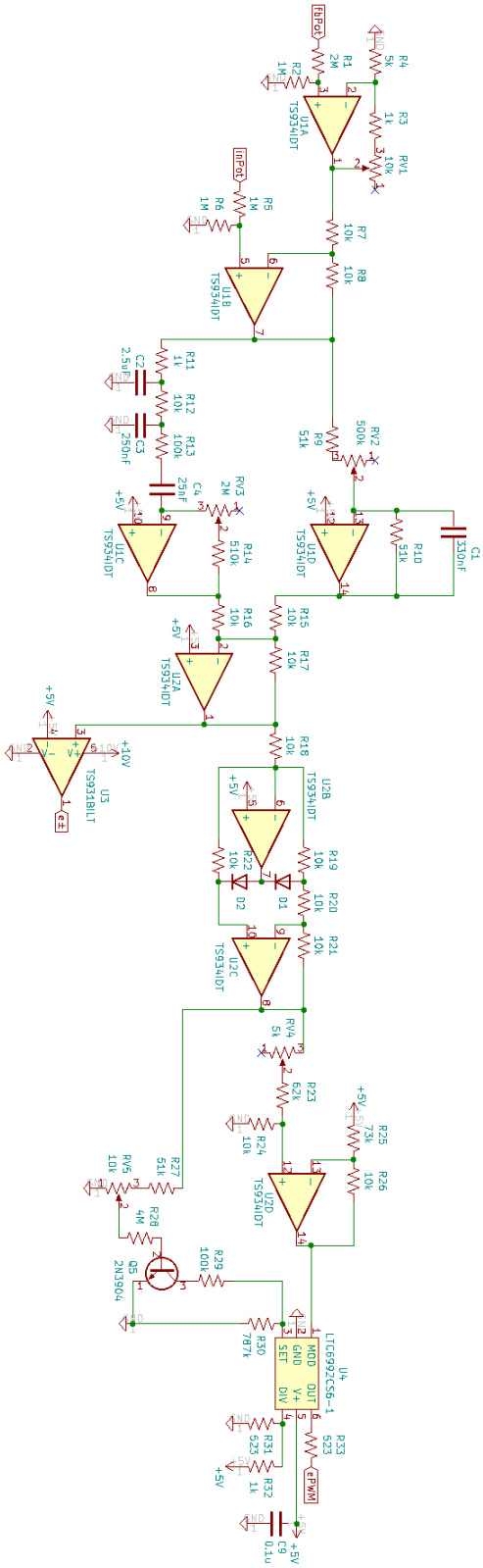

Appendix D: MATLAB Code

Full System Simulation

```
function PaddleshifterControllerSimulation
clear all

%% Simulation Parameters
n = 5;              %order of system
x0 = zeros(n,1);    %reserves x0 for IC of open system
x0(1) = 0;          %initial conditions for pos
x0(2) = 0;          %initial conditions for vel
x0(3) = 100;              %initial conditions for pressure
x0(4) = 300;              %initial conditions for temp
x0(5) = 0;                %initial conditions for udot

Tinit = 0;          %initial time
Tfinal= 0.7;        %final time
Tstep=0.001;        %time step (must use consistent step b/c of friction
model)

%% System Variables
Acyl=386;   %mm^2
Kcyl=3.4;     %n/mm
Mcyl=0.151;  %kg
Ta=300;     %K
Pin=926;    %kPa
Patm=100;   %kPa
h=150;     %W/m^2K
Aw=1670;    %mm^2
Tw=300;     %K
k=1.4;
C=900;      %mm^2
R=287;      %Nm/kgK
CdA=1.55;   %mm^2
DCmin=0.007;    %minimuum duty cycle before flow occurs
DCgain=1.01;    %injector gain from DC
Kp=0.75/16;    %1/mm  0.75, with no Kd, this needs to be about 0.2
Kd=0.025/16;  %s/mm  0.025
filt1=63;       %kd filter freq, hz
filt2=63;
filt3=63;
filt1=1/(2*pi*filt1); %time constant
filt2=1/(2*pi*filt2);
filt3=1/(2*pi*filt3);

fc=2.2;     %N
sumF=0;     %sum of forces except friction
fric=0;     %fricitonal force applied
Vmin=1000*fc*Tstep/Mcyl; %mm/s
Fstate=0;   %used for DAQ & troubleshooting

%% I/O Physcial Limits/Commands
%for step or ramp selection go to odefun and uncomment/comment section needed
%for initial vals, change x(1) at top and change u below.
zmax=16;    %mm
```

```
ugain=zmax/0.5;  %mm/s gain used for ramp input,
u0=0;
u=u0;
udot=ugain;

%          T     u z     v     a Pcv   Tcv   DC Fpr_up Fpr_dn Vcv Vdot Mcv
mdotin mdotout sumF   Fstate
results = [Tinit u x0(1) x0(2) 0 x0(3) x0(4) 0  0      0      C   0    0   0
0       sumF   Fstate];

%% Simulation
tSpan =[Tinit:Tstep:Tfinal];
%integrate
[t,x]=ode45(@DerFun,tSpan,x0);
%plot output
colororder({'k','k'})
yyaxis left
plot(results(:,1),results(:,2),'k-','LineWidth',2.5)     %input for ramp
input
hold on
plot(t,x(:,1),'b-','LineWidth',2.5)     %cyl disp in mm
ylim([-5 20])
plot(t,x(:,2)/100,'r-','LineWidth',2.5)     %cyl vel in mm/s (scaled by 1/10
to fit in window)
ylabel('Position (mm),   Velocity (0.01*mm/s)','FontSize', 14)
title('Paddleshifter Simulation Ramp Input FSI/500ms', 'FontSize', 14)
yyaxis right
plot(t,x(:,3)-100,'k-','LineWidth',2.5)      %Pcv  converted to gauge
plot(t,x(:,4)-273,'g-','LineWidth',2.5)      %Tcv converted to C
ylim([0 200])
legend({'Input','Position','Velocity','Pressure','Temperature'},'FontSize',10
,'Location','northwest')
grid
xlabel('Time (s)','FontSize',14)
ylabel('Pressure (kpa-g),   Temperature(°C)','FontSize', 14)

writematrix(results);

%% Derivatives and Switch/Cases
function Dx=DerFun(t,x)
Dx = zeros(n,1);
%% Input Parameters
Dx(5)=u;

%step Input
%u=0;
%udot=0;

%Ramp input
u=u0+ugain*t;
if(u>=zmax)
    u=zmax;
    udot=0;
elseif(u<=0)
        u=0;
        udot=0;
end
```

```
%% DC Calc & Saturation
DC=Kp*(u-x(1))+Kd*(x(5)-x(2))/(filt3*(x(5)-x(2))+1)*1/(filt2*(x(5)-
x(2))+1)*1/(filt1*(x(5)-x(2))+1);
%injector output
if abs(DC)<DCmin
    DC=0;
else
    DC=DC*DCgain;
end
%sat
if DC>1
    DC=1;
end
if DC<-1
    DC=-1;
end

%% Pressure Ratio Choking & PR FUNC. CALC
if (x(3)/Pin)<0.5
    fpr_up=0.5;
else
    fpr_up=sqrt((x(3)/Pin)-(x(3)/Pin)^2);
end

if Patm/x(3)<0.5
    fpr_dn=0.5;
else
    fpr_dn=sqrt((Patm/x(3))-(Patm/x(3))^2);
end

%% Mechanical SS Eqns
Dx(1)=x(2);
Dx(2)=(1/Mcyl)*((x(3)-Patm)*Acyl-1000*Kcyl*x(1)-1000*fric);

 %% P and T Calculated Vars & mdot direction
Vcv=Acyl*x(1)+C;
Vdot=Acyl*x(2);
Mcv=(x(3)*Vcv/(R*x(4)))/1000000;
mdotin=DC*CdA*Pin*sqrt(2/(R*x(4)))*fpr_up/1000;
mdotout=DC*CdA*x(3)*sqrt(2/(R*Ta))*fpr_dn/1000;
if DC>0
    mdotout=0;
elseif DC<0
    mdotin=0;
end

%% P & T SS Eqns
Dx(3)=x(3)*((k*(mdotin*Ta/(Mcv*x(4))+mdotout/Mcv))-((k-1)*(x(4)-
Tw)*h*Aw/(x(3)*Vcv))-(k*Vdot/Vcv));
Dx(4)=x(4)*(((mdotin/Mcv)*(k*Ta/x(4)-1))-(mdotout*(k-1)/Mcv)-((k-1)*(x(4)-
Tw)*h*Aw/(x(3)*Vcv))-((k-1)*Vdot/Vcv));

%% Friction Switch/Case
sumF=((x(3)-Patm)*Acyl-Kcyl*x(1)-Mcyl*Dx(2))/1000;
if abs(x(2))>Vmin
    fric=fc*sign(x(2));
```

```
    Fstate=1;
else
    if abs(sumF)<fc
        fric=sumF;
        Fstate=2;
    else
        fric=fc*sign(sumF);
        Fstate=3;
    end
end

%% DAQ & Troubleshooting
results= [results;[t u x(1) x(2) Dx(2) x(3) x(4) DC fpr_up fpr_dn Vcv Vdot
Mcv mdotin mdotout sumF Fstate]];

disp(['time ', num2str(t), ' pos ', num2str(x(1)),' query ', num2str(x(1))]);
end
end
```

Injector Simulation

```
function Injector_Sim_OneCycle
clear all

%% Simulation Parameters
n = 3;              %order of system
x0 = zeros(n,1);    %reserves x0 for IC of open system
x0(1) = 0;          %initial conditions for open pos
x0(2) = 0;          %initial conditions for open vel
x0(3) = 0;          %initial conditions for current

freq=200;           %Inj driving freq in Hz
cycle=1/freq;
DC=0.085;            %DC of elec. driving frequency in Hz
Tinit = 0;          %initial time
Tstep=cycle/200;

Icc=1.2;            %Amps, constant current value
Vin=12;             %Voltage, input voltage

%% System Variables mechanical movement inside injector
L=0.00514;          %Henrys,     inj inducance
R=2.4;              %Ohms,       inj resistance
m=1.57/1000;        %grams->kg,  mass of shuttle
k=3.03*1000;        %N/mm ->N/m, spring rate of inj spring
Fp=6.54;            %N,          preload force from injector spring
delP=90*6895;       %psi  ->Pa,  Upstream Pressure, will change to SS var
later
A1=1.82/1000000;    %mm^2 ->m^2, SEALING area of injector, not orifice
xmax=0.08/1000;     %mm   ->m,   max x travel of shuttle
xcrit=0.02/1000;    %mm   ->m,   critical disp of shuttle to allow airflow,
acting as bool
```

```
Ibreak=(delP*A1+Fp)/18.7;%Breakaway current required to overcome preload and
pressure
Ihold=Ibreak+k*xmax;

%% Simulation
tSpan =[Tinit:Tstep:cycle];
[t,x]=ode23(@DerFun,tSpan,x0);

%% Averaging normalized flow
for i=1:1:length(t)
   if x(i,1)>xcrit
       mdot(i)=1;
   else
       mdot(i)=x(i,1)/xcrit;
   end
end
mean(mdot)
plotTitle=strcat('Injector Simulation, DutyCycle= ',num2str(100*DC),'%, Freq=
',num2str(freq),'Hz, Vin=', num2str(Vin),'V');
%plot output
colororder({'k','k'})
plot(t,10000*x(:,1),'b','LineWidth',2.5)     %inj disp in mm
hold on
plot(t,x(:,2),'r-','LineWidth',2.5)          %inj vel in m/s
plot(t,mdot,'g-','LineWidth',2.5)               %mdot
ylabel('Response (µm, mm/s, UD, A)','FontSize', 14)
ylim([-0.75 1.25])
yticks(-0.75:0.25:1.25)
title(plotTitle, 'FontSize', 14)
plot(t,x(:,3),'k-','LineWidth',2.5)          %inj current in Amperes
legend({'Shuttle Position','Shuttle Velocity','Norm.
MDot','Current'},'FontSize',12,'Location','southeast')
xlim([0 cycle])
grid
xlabel('Time (s)','FontSize',14)

%% Derivatives and Switch/Cases
function Dx=DerFun(t,x)
Dx = zeros(n,1);

%% Mechanical Dynamic Equations
if x(1)<=xmax || x(3) < Ibreak %in motion
    Dx(1) = x(2);
    if(x(1)<xcrit)
        Dx(2) = (-1/m)*(k*x(1)+Fp+delP*A1-InjForce(x(3),x(1)) );
    else
        Dx(2) = (-1/m)*(k*x(1)+Fp        -InjForce(x(3),x(1)) );
    end
elseif x(1)>xmax && x(3)>=Ihold %upper mech. stop
    Dx(1)=10*(xmax-x(1));
    Dx(2)=1000000*(0-x(2));
end
if x(1)>xmax && x(2)>0.01 %case for small DC, high voltage where current is
@0 by the time the mass finally cathes up
    Dx(1)=10*(xmax-x(1));
    Dx(2)=1000000*(0-x(2));
end
```

```
if x(1)<0 && x(3) < Ibreak %lower mech. stop
    x(1)=0;
    Dx(1) = 1000000*(0-x(1));
    Dx(2) = 1000000*(0-x(2));
end

%% determining drive state / Input command
tempCount=t;
while (tempCount>cycle)
    tempCount=tempCount-cycle;
end
%% drive pulses condition
if tempCount<cycle*DC
    if x(3)<Icc
        Dx(3) = (Vin-x(3)*R)/L;     %on condition
    else
        Dx(3) = 1000000*(Icc-x(3)); %constant current
    end
else
    Dx(3) = -1000000*x(3);          %off condition
end

end
%% EM Force Function
function Fem=InjForce(i,x) %current on coil in A, disp of plunger in m,
returns Newtons
Fem= 18.7*i;
Fsat=12.5-46.2*1000*x;
if Fem>Fsat
    Fem=Fsat;
end
end
end
```

Appendix E: Paddle-shifter Code

```
//INPUT PINS
const int inPot      = A5; //Pot on wheel
const int fbPot      = A6; //pin input
const int gearPos    = A7; //pin for analog gear position input
const int inShiftUp  =  2; //button in wheel, upshift
const int inShiftDn  =  3;
const int launch     =  4; //pin for launch control command

//OUTPUT PINS
const int pe3        = 13; //pin to pe3 for rpm hold
const int ignCut     =  8; //pin for cut ign on upshift
const int outShiftUp = 11; //to Solenoid for Upshift,
const int outShiftDn = 12;
const int ntrlLim    =  5;

//LAUNCH OVERRIDE PINS
const int biteOut    =  9; //output for bite point val
const int biteSW     =  7; //output controls bite Switch
const int launchOut  =  6; //output for launch rate val
const int launchSW   = 10; //output controls launch Switch

boolean latch   = false;
boolean holdRPM = false;
boolean latchRPM = false;
int   bitePoint = 70;  //point just before clutch  bite 255=5V, 0=10V,
int   holdTime  = 900;  //time to hold rpm in ms
int   lnchEror  = 40;  //error used during launch for clutch release 255=1V, 0=0V
int   clutchCom = 70; //this variable is what is applied to clutch position
int   prevCC=70;     //previous value of clutch command

int  inVal = 0; //value for clutch comm
int  fbVal = 0; //value for clutch pos

long unsigned int t1 = 0; //shifts
long unsigned int t2 = 0; //nuetral
long unsigned int t3 = 0; //shift delay between
long unsigned int t4 = 0; //counter for reqeusts
long unsigned int t5 = 0; //counter for launch control 2step

int  cutDelay  = 50; //Delay between sending signal to upshit and asking to cut ignition
int  st       = 80; //Shift Time in ms
int  ntrl     = 8;   //Nuetral Shift time in ms
int  sDelay   = 100; //delay between shifts to allow cylinder to retract ot center pos.
int  reqDelay  = 20;  //delay between possible requests
```

```
boolean rset = false;
int greq = 10; //gear request, 10 is no change

void setup() {
 Serial.begin(9600);

 pinMode(inPot, INPUT);
 pinMode(fbPot, INPUT);
 pinMode(inShiftUp, INPUT_PULLUP);
 pinMode(inShiftDn, INPUT_PULLUP);
 pinMode(launch, INPUT_PULLUP);

 pinMode(pe3, OUTPUT);
 pinMode(outShiftUp, OUTPUT);
 pinMode(outShiftDn, OUTPUT);
 pinMode(biteOut, OUTPUT);
 pinMode(biteSW, OUTPUT);
 pinMode(launchOut, OUTPUT);
 pinMode(launchSW, OUTPUT);
 pinMode(ignCut, OUTPUT);

 clutchCom=bitePoint;
 prevCC=clutchCom;
 analogWrite(biteOut, clutchCom);
 analogWrite(launchOut, lnchEror);
 digitalWrite(ignCut, HIGH);
}

void loop() {

 //LAUNCH CONTROL

 inVal = map(analogRead(inPot), 390, 1023, 0, 1023);
 fbVal = map(analogRead(fbPot), 0, 1023, 0, 1023);
 digitalWrite(ntrlLim,LOW);
 if (digitalRead(launch) == LOW)
 {
  latch = true;
  t5 = millis();
 }
 //abort if timeout of 1.3sec from button release, if clutch pos is all the way out, or if clutch
request is farther in than clutch pos
 if (millis() - t5 > 1300 || fbVal < 50 )
 {
  latch = false;
```

```
  latchRPM = false;
}
if (latch)
{
  if(inVal<800) //only move clutch to bitePoint if you have clutch out.
     digitalWrite(biteSW, HIGH);
  else
     digitalWrite(biteSW, LOW);

  if (digitalRead(launch) == HIGH)
  {
   digitalWrite(launchSW, HIGH);
   clutchCom=255;
  }

  if (digitalRead(launch) == HIGH && !latchRPM)
  {
   latchRPM = true;
   holdRPM = true;
   t5 = millis();
  }
}
else
{
  digitalWrite(biteSW, LOW);
  digitalWrite(launchSW, LOW);
  clutchCom=bitePoint;
}
if (millis() - t5 > holdTime)
  holdRPM = false;
if (holdRPM)
  digitalWrite(pe3, HIGH);
else
  digitalWrite(pe3, LOW);

if(prevCC != clutchCom)
{
  analogWrite(biteOut, clutchCom);
  prevCC=clutchCom;
}



//SHIFTER

//Gear Request Counter
```

```
 if (!rset)
 {
  if ((digitalRead(inShiftUp) == LOW) && (digitalRead(inShiftDn) == HIGH))
  {
   greq++;
   rset = true;
   t4 = millis();
  }
  else if ((digitalRead(inShiftUp) == HIGH) && (digitalRead(inShiftDn) == LOW))
  {
   greq--;
   rset = true;
   t4 = millis();
  }
 }
 if ((digitalRead(inShiftUp) == HIGH) && (digitalRead(inShiftDn) == HIGH) && (millis() -
t4) >= reqDelay)
  rset = false;


 if (greq < 10 && (millis() - t3) >= sDelay) //downshift condition
 {
  if (t1 == 0)
   t1 = millis();

  if ((millis() - t1) < st) //rising edge and during cond
  {
   digitalWrite(outShiftDn, HIGH);
  }
  else if (((millis() - t1) >= st)) //falling edge
  {
   digitalWrite(outShiftDn, LOW);
   greq++;
   t1 = 0;
   t3 = millis();
  }
 }
 else if (greq > 10 && (millis() - t3) >= sDelay) //upshift condition
 {
  if (t1 == 0)
   t1 = millis();
  if(!latch)
  {
   if ((millis() - t1) < st) //rising edge and during cond
   {
    digitalWrite(outShiftUp, HIGH);
```

```
      if((millis() - t1) >= cutDelay)
      {
        digitalWrite(ignCut, LOW);
      }
     }
     else if (((millis() - t1) >= st)) //falling edge
     {
      digitalWrite(outShiftUp, LOW);
      digitalWrite(ignCut    , HIGH);
      greq--;
      t1 = 0;
      t3 = millis();
     }
    }
    else //ntrl condition for cars w/o gear position sensor
    {
     if ((millis() - t1) < ntrl) //rising edge and during cond
     {
      digitalWrite(outShiftUp, HIGH);
     }
     else if (((millis() - t1) >= ntrl)) //falling edge
     {
      digitalWrite(outShiftUp, LOW);
      greq--;
      t1 = 0;
      t3 = millis();
     }
    }
   }
   else if (greq == 10) //Reqs out of bounds catch
   {
    digitalWrite(outShiftDn, LOW);
    digitalWrite(outShiftUp, LOW);
    t1 = 0;
    t2 = 0;
   }

}
```

References

1. "2018 Lincoln FSAE Competition Results." Lincoln, 2018.

2. "Analog Position Sensor and NCMC Cylinder Datasheets." *Smcusa.com*, SMC.

3. Chalmela, Rahul J. "Electro-Pneumatic Shifting and Servo Control of a Clutch for a FSAE Racecar." *University of Texas Arlington*, 2017.

4. "Formula SAE Rules 2022 Version 1." *Fsaeonline.com*, SAE International, 2021.

5. "LTC6992." *Datasheet and Product Info | Analog Devices*, Nov. 2019, https://www.analog.com/en/products/ltc6992-1.html.

6. Nise, N.S. "11.4 Design via Frequency Response: Lead Compensation." *Control Systems Engineering*, 7th ed., John Wiley & Sons, New York, NY, 2011, p. 626.

7. Woods, Robert L, and Kent L Lawrence. *Modeling and Simulation of Dynamic Systems*. Prentice Hall, 1997.

8. Woods, Robert L. *Control System Components*. Course Work, ME 5341.

9. Woods, Robert L. "Coulomb Friction Between Two Moving Bodies Including Static and Dynamic Motion." Feb. 23 2005. Print.

10. Woods, Robert L. Personal Correspondence. *"Compressible Continuity Equation."* 2021.

11. Woods, Robert L. Personal Correspondence. *"Governing Equations for Pneumatic System Dynamics."* 2021